



THESIS

1  
(1990)



This is to certify that the

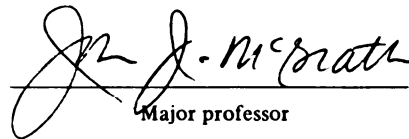
thesis entitled

DEVELOPMENT AND EVALUATION of  
3-D OPTICAL SECTIONING FOR THE INVESTIGATION OF  
FIBER ORIENTATION DISTRIBUTION IN INJECTION-MOLDED,  
FIBER REINFORCED THERMOPLASTICS  
presented by

Bin Lian

has been accepted towards fulfillment  
of the requirements for

M.S. degree in Mechanical Engineering

  
Major professor

Date 11/17/94

**LIBRARY**  
**Michigan State**  
**University**

PLACE IN RETURN BOX to remove this checkout from your record.  
 TO AVOID FINES return on or before date due.

DATE DUE	DATE DUE	DATE DUE
_____	_____	_____
_____	_____	_____
_____	_____	_____
_____	_____	_____
_____	_____	_____
_____	_____	_____
_____	_____	_____

MSU Is An Affirmative Action/Equal Opportunity Institution

c:\pic\datedue.pm3-p.1

**DEVELOPMENT AND EVALUATION OF  
3-D OPTICAL SECTIONING FOR THE INVESTIGATION OF  
FIBER ORIENTATION DISTRIBUTIONS IN INJECTION-MOLDED,  
FIBER REINFORCED THERMOPLASTICS**

**By**

**Bin Lian**

**A THESIS**

**Submitted to  
Michigan State University  
in partial fulfillment of the requirements  
for the degree of**

**MASTER OF SCIENCE**

**Department of Mechanical Engineering**

**1994**



# ABSTRACT

## DEVELOPMENT AND EVALUATION OF 3-D OPTICAL SECTIONING FOR THE INVESTIGATION OF FIBER ORIENTATION DISTRIBUTIONS IN INJECTION-MOLDED, FIBER REINFORCED THERMOPLASTICS

By

Bin Lian

Calibrations and measurement accuracy estimates were carried out to evaluate and improve the novel technique developed at MSU for the investigation of the three-dimensional fiber orientation distributions for fiber reinforced thermoplastics. Comparison of the results given by optical sectioning and surface ellipse methods suggested no significant difference of these two methods. This new method is accurate, non-destructive, and much faster than the cut and polish method. Appropriate statistical descriptions for the second order orientation tensor components and their corresponding errors were also developed. Error estimates were performed to identify the potential sources of errors which contribute to the measurement uncertainty. The injection apparatus is shown to produce specimens under industrially relevant conditions and the imaging and analysis software can provide accurate and detail information describing fiber orientation distribution rapidly. The influences of processing conditions on the FODs were also defined.

**To my wife and my parents**

## **Acknowledgments**

I would like to express my deepest appreciation and regards to my advisor Dr. John McGrath for his continued support and guidance throughout the length of this project. Also I would like to thank Dr. Jeff Wille for the invaluable discussions and insights. Thanks are due to several exchange students from Germany, Armin Noethe, Jan Ladewig and Nils Schoche for their great assistance. I must thank Dr. Gilliland of the Statistics Department for the insightful comments about the statistical description.

I am thankful for the support of Michigan State University and the State of Michigan Research Excellence Fund awarded through the Composite Materials and Structure Center.

## **Nomenclatures**

$a_{ij}$	second order orientation components
$b$	half height of mold cavity ( $H/2$ )
$Br$	Brinkman Number
$\mathbf{p}$	fiber orientation vector
$d$	fiber diameter
$Gz$	Graetz Number
$H$	height of mold cavity
$k$	thermal conductivity
$l$	fiber length
$L$	length of mold cavity
$n$	refractive index
$Pn$	Pearson Number
$t_{fill}$	time required to fill the mold
$U$	average flow velocity
$x$	flow direction coordinate (zero at gate)
$y$	transverse (in plane) coordinate (zero at vertical midplane)
$z$	optical axis coordinate (zero at horizontal midplane)

## **Greek**

$\alpha$       thermal diffusivity

$n$       power index of power law model ( $\eta = m\dot{\gamma}^{n-1}$ )

$\eta$       polymer melt viscosity

$\theta$       Eulerian angle with respect to z-axis

$\phi$       Eulerian angle in x-y plane with respect to x axis

$\Psi(\theta, \phi)$  orientation distribution function

# Table of Contents

<b>List of Tables</b> .....	i
<b>List of Figures</b> .....	ii
<b>1. Introduction</b> .....	1
<b>1.1 Injection Molding of Short Fiber Reinforced Thermoplastics.</b>	1
1.1.1 Industrial Injection Molding Technique for Polymer Processing...	1
1.1.2 Concept of Plastic Reinforcing .....	3
1.1.3 Short Fiber Reinforced Thermoplastics .....	4
<b>1.2 Mathematical Description of FODs</b> .....	5
<b>1.3 Investigation Tools for Studies of FODs</b> .....	8
1.3.1 Traditional Methods .....	8
1.3.2 Optical Sectioning .....	10
<b>1.4 Optical Sectioning for SF RTP Research</b> .....	10
1.4.1 Basic Concepts of Optical Sectioning .....	10
1.4.2 Advantages of Optical Sectioning Method .....	12
1.4.3 Injection Molding Apparatus .....	15

1.4.4	Imaging Apparatus .....	16
1.4.5	Image Processing Software .....	17
1.4.5.1	3-D Thinning .....	17
1.4.5.2	3D-FODAS - Extraction of FOD Information .....	19
1.4.5.3	FIBOR - Ellipsoid Visualization .....	20
1.4.5.4	PSEUDO - Generation of Images with Specified FODs..	21
1.4.6	Some Perspectives for the Development of the Optical Sectioning Technique .....	21
<b>2.</b>	<b>Calibration.....</b>	<b>23</b>
2.1	Calibration Using Pseudo-data.....	23
2.2	Single Fiber Calibration.....	24
2.3	Orthogonal Specimen.....	25
<b>3.</b>	<b>Comparison of FODs Determined by Optical Sectioning and Cut/Polish Method.....</b>	<b>27</b>
<b>4.</b>	<b>Image Processing.....</b>	<b>29</b>
4.1	Image “Crushing” to Remove Fiber Clumps.....	29
4.2	Influence of Non-Uniform Voxel Sizes on FODs.....	31
<b>5.</b>	<b>Error Estimates and Analyses.....</b>	<b>33</b>

<b>5.1 Motivation.....</b>	<b>33</b>
<b>5.2 Possible Sources of Errors.....</b>	<b>34</b>
<b>5.3 Confidence Limit on FODs - Standard Error of Tensor       Components .....</b>	<b>37</b>
<b>5.4 Estimation of Measurement Error.....</b>	<b>40</b>
 <b>6. Influence of Processing Parameters on FODs.....</b>	 <b>43</b>
<b>6.1 Injection Molding Process.....</b>	<b>43</b>
<b>6.2 Processing Parameter Influences on the FODs.....</b>	<b>45</b>
 <b>7. Results and Discussions.....</b>	 <b>49</b>
<b>7.1 Calibrations.....</b>	<b>49</b>
7.1.1 Pseudo Data Calibration.....	49
7.1.2 Results from Orthogonal Scans.....	50
<b>7.2 Comparisons of FOD Results from Optical Sectioning and       Cut/Polish Method.....</b>	<b>54</b>
<b>7.3 Imaging Processing.....</b>	<b>58</b>
7.3.1 Fiber Clumps “Crushing”.....	58
7.3.2 Results of Influence of Non-Uniform Voxel Size.....	61
<b>7.4 Estimates of Measurement Errors.....</b>	<b>63</b>
<b>7.5 Results of Influence of Processing Parameters on FODs.....</b>	<b>65</b>
7.5.1 Experimental Results of Influence of Processing Parameters on	



FODs .....	65
7.5.2 Results of Simulation of FOD Evolution During Mold Filling	
Process .....	68
<b>8. Conclusions and Recommendations for Future work....</b>	<b>74</b>
<b>8.1 Calibrations.....</b>	<b>74</b>
<b>8.2 Image Processing.....</b>	<b>75</b>
<b>8.3 Statistical Analysis.....</b>	<b>76</b>
<b>8.4 Experimental Investigations of FODs.....</b>	<b>76</b>
<b>8.5 Other Considerations.....</b>	<b>77</b>
<b>Appendices.....</b>	<b>79</b>
<b>A. Ratio Approach for Standard Error Calculation.....</b>	<b>79</b>
<b>B. Specimen Geometry.....</b>	<b>80</b>
<b>List of References.....</b>	<b>81</b>

## **List of Tables**

1. Refractive Indices of Glass .....	13
2. Refractive Indices of Transparent Industrial Polymers and Possible Matches with Glass.....	14
3. Operating Range of Injection Molding Apparatus .....	16
4. Tensor Components and Unit Vectors of Major Axes of the Ellipsoids (Tessellation Order 2).....	52
5. Difference in Directions Between Individual Scans and the Mean.....	53
6. Comparison of Tensor Components for Scans Using Different Voxel Sizes.....	62
7. Comparison of Angle Differences from the Mean Direction for Scans Using Different Voxel Sizes.....	63
8. Comparison of Experimental Uncertainty and Theoretical Estimates.....	64
9. Error Contribution in Percentage.....	64

## List of Figures

1.	Schematic of Injection Molding Apparatus .....	2
2.	Determination of FODs by Cut/Polish Method .....	9
3.	Schematic of Optical Sectioning .....	11
4.	A 2-D Image: From Which 3-D Image is Constructed.....	12
5.	Injection Molding Apparatus .....	15
6.	Imaging System .....	17
7.	3-D Thinning .....	18
8.	Visualization of FOD by 3D-FODAS .....	20
9.	Visualization of Second Order Tensor.....	21
10.	Orthogonal Scans.....	26
11.	Scan Locations for Optical Sectioning and Cut/Polish.....	27
12.	Sample Image with Fiber Clumps and the Schematic of the Image Preprocessing for Fiber Clump Removal.....	30
13.	Sampling Error versus Number of Tracer Fibers.....	39
14.	3 x 1 Repeated Scans in the Shell and Core layers.....	42
15.	Formation of Solid Boundary Layer and Velocity Profile.....	44
16.	Visualization of Result from the Four Orthogonal Scans.....	51
17.	t-distribution for n=4.....	55

18.	Comparison of $\langle a_{11} \rangle$ and $\langle a_{33} \rangle$ Given by Optical Sectioning and Cut/Polish Method and the Corresponding Significance Level of Difference (Sample no8).....	56
19.	Comparison of $\langle a_{11} \rangle$ and $\langle a_{33} \rangle$ Given by Optical Sectioning and Cut/Polish Method and the Corresponding Significance Level of Difference (Sample ob7).....	57
20.	Effect of the Preprocessor for Real Images with Fiber Clumps.....	60
21.	Influence of Temperature and Injection Speed on FODs.....	66
22.	Material Effect on FODs.....	67
23.	Material Influence on FODs for PMMA and Nylon 6/6.....	71
24.	Evolution of FODs for $T_{\text{melt}}$ (PMMA) at 260C.....	72

## **Chapter 1**

# **Introduction**

### **1.1 Injection Molding of Short Fiber Reinforced Thermoplastics**

#### **1.1.1 Industrial Injection Molding Technique for Polymer Processing.**

Injection molding thermoplastic technology has a long history of more than one century. It is gaining more attention and has acquired an increasing share of the manufacturing industry. As one of the most common technologies in the polymer processing industry, weight saving, remoldability, great surface appearance and low cost of the finished parts give this technique many advantages over the traditional metal casting method. Capable of high volume of production, good product quality consistency and low labor intensity are several other important technology niches for today's successful manufacturing operation. These factors make injection molding a practical choice for plastic

part production, among other manufacturing technologies. Recyclability, as one of the major environmental concerns, also pushes people to switch to the more environmental friendly plastic products among which a large fraction are made by injection molding.

There has been tremendous progress in injection molding technique since the first prototype was built. Reaction injection molding (RIM), resin transfer molding (RTM) and many other modifications and applications are just a few examples of technologies which grew out of the basic injection molding concept. Figure 1 shows the schematic of a simple injection molding machine.

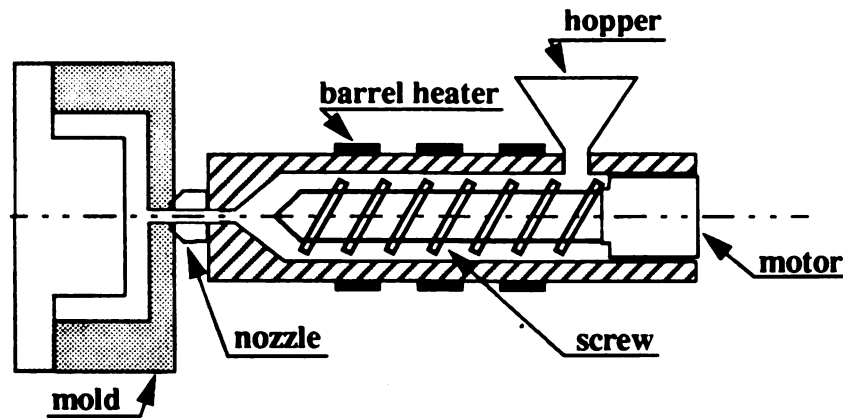


Figure 1. Schematic of Injection Molding Apparatus.

Because of high viscosity, polymer melts cannot be poured into the mold. They must be injected into the mold cavity by applying large forces with a plunger. Moreover, once the mold is filled with melt solidification takes place where the hot melt meets the cold wall. Therefore an additional amount of

melt must be packed into the mold to offset polymer shrinkage during cooling process and to achieve an accurate reproduction of the mold cavity geometry.

Injection molding equipment consists of two major parts: the injection unit and the clamping unit. The function of the former is to melt the polymer and inject it into the mold, whereas the clamping unit holds, opens and closes the mold automatically, and ejects the finished product. Present injection units are almost exclusively of the in-line reciprocating screw type. The screw both rotates and undergoes axial reciprocal motion. When it rotates, it acts like a screw extruder, melting and pumping the polymer. When it moves axially, it acts like an injection plunger. The screw is, in general, rotated by a hydraulic motor and its axial motion is activated and controlled by a hydraulic system (Tadmor and Gogos, 1979).

### **1.1.2 Concept of Plastic Reinforcing**

Plastic is not as strong as metal on a strength per unit volume basis, but the incorporation of fibers into polymer matrices increases the strength and stiffness as well as the heat deflection temperature (the temperature above which the material deforms significantly under load). Fiber reinforcement also increases the flexural modulus to a magnitude comparable to that of traditional construction materials. Other advantages of reinforced plastics include

better performance in creep and temperature resistance, as well as reduced thermal expansion and mold shrinkage. Among all these advantages, cost effectiveness and its environmental friendly nature are also important reasons to use fiber reinforced plastics as substitutes for metals. However, the addition of brittle fiber materials can reduce the impact strength of thermoplastics (Rayson, McGrath and Collyer, 1986).

In a typical industrial manufacturing process for fiber reinforced thermoplastics, the reinforcing agents which can take on the form of fibers or flakes are mixed with matrix materials and fed into the extrusion machine, where the mixture is heated and extruded and cut into small pellets. The pellets can be injection or compression molded into finished products in the same manner as traditional unfilled plastics.

### **1.1.3 Short Fiber Reinforced Thermoplastics**

Among all the available composite fabrication techniques, chopped short fiber reinforced thermoplastic (SF RTP) injection molding is the most feasible for high volume production. It has the obvious advantages of excellent reproducibility and low labor intensity which means low cost. Normal injection molding machines for plastics can be used for injection molding of filled plastics. However, sometimes it might be necessary to use special screws and barrels to



prevent excessive wear of the machinery since some glass fibers can be abrasive.

The outstanding mechanical properties of reinforced plastics stem from the effective load transfer from the external stress to the reinforcing materials. For short fiber reinforced thermoplastic composite, care must be taken to ensure that the fiber aspect ratio must be higher than the critical aspect ratio to retain the objective of reinforcing.

The performance of fiber reinforced thermoplastic products not only depends on how much reinforcing material is inside the composite (volume fraction), it is also determined by the orientation of the fibers which can produce a highly anisotropic material. It is necessary to describe the properties in terms of volume fraction and fiber orientation distribution (FOD). For a fixed glass content, the FOD information becomes critical because the FOD will be related to various processing parameters and to bulk properties. Based upon this information, decisions about the processing can be made to meet the criteria of the design objective.

## **1.2 Mathematical Description of FODs**

After the fiber orientation distribution information has been extracted from

the measurement, we need to describe this information. One obvious choice is the analytical or numerical distribution function, which gives a complete description of FODs. The probability of a fiber being oriented between the angle  $\theta_1$  and  $(\theta_1 + d\theta)$ ,  $\phi_1$  and  $(\phi_1 + d\phi)$ , and having a length between  $L_1$  and  $(L_1 + dL)$  is

$$P(\theta_1 \leq \theta \leq \theta_1 + d\theta, \phi_1 \leq \phi \leq \phi_1 + d\phi, L_1 \leq L \leq L_1 + dL) = \psi(\theta_1, \phi_1, L_1) \sin\theta_1 d\theta d\phi dL \quad [1]$$

$$\text{where } \int \int_{PL} \psi(\vec{P}, L) (dL) d\vec{P} = 1 \quad .$$

The distribution function approach has been found to be workable in two dimensional cases provided some assumptions are made to simplify the problem. It is impractical to apply it to three dimensional cases in relation to both computer power and space needed to store the data. Advani and Tucker (1987) proposed a tensor description for the fiber orientation distributions which has been widely accepted. The orientation tensors are created by forming dyadic products of the direction vector  $\mathbf{p}$  and integrating over all directions, weighting the product with the distribution function.

$$a'_{ijk...l} = \frac{\int \int_{LP} p_i p_j p_k \dots p_l L^t \psi(\vec{p}, L) d\vec{p} dL}{\int \int_{LP} L^t \psi(\vec{p}, L) d\vec{p} dL} \quad [2]$$

where  $t=0$  represents a number-average orientation distribution, and  $t=1$  represents a weight-average orientation distribution. Since the distribution func-

tion has even polarity, i.e.,  $\psi_p(\vec{p}, L) = \psi_p(-\vec{p}, L)$ , all the odd-rank tensors are zero. This approach is analogous to using Taylor's series (or polynomials) to approximate a complex function. The higher order tensors provide the better approximations. Advani and Tucker's review (1991) showed that only the second and fourth-rank tensors are needed for most purposes, and usually only the second-rank tensor is used in the prediction of FODs. However a closure law has to be incorporated into the equation to reduce the fourth order terms to second order terms.

The second order tensor can be written as following:

$$\langle a_{11} \rangle = \langle \sin^2 \theta \cos^2 \phi \rangle \quad [3]$$

$$\langle a_{12} \rangle = \langle \sin^2 \theta \cos \phi \sin \phi \rangle \quad [4]$$

$$\langle a_{13} \rangle = \langle \sin \theta \cos \theta \cos \phi \rangle \quad [5]$$

$$\langle a_{21} \rangle = \langle a_{12} \rangle \quad [6]$$

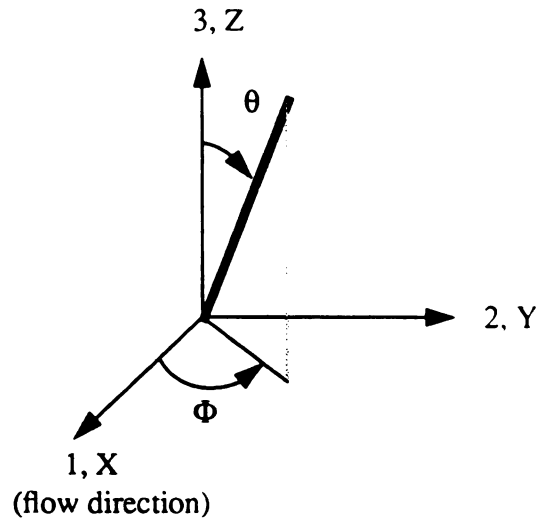
$$\langle a_{22} \rangle = \langle \sin^2 \theta \sin^2 \phi \rangle \quad [7]$$

$$\langle a_{23} \rangle = \langle \sin \theta \cos \theta \sin \phi \rangle \quad [8]$$

$$\langle a_{31} \rangle = \langle a_{13} \rangle \quad [9]$$

$$\langle a_{32} \rangle = \langle a_{23} \rangle \quad [10]$$

$$\langle a_{33} \rangle = \langle \cos^2 \theta \rangle \quad [11]$$



where each tensor component is the length weighted average of all the fibers in the population, defined as the following:

$$\langle a_{ij} \rangle = \frac{\sum_k l_k \cdot a_{ij}^k}{\sum_k l_k} \quad [12]$$

where  $l_k$  is the length of the  $k$ th fiber and  $a_{ij}^k$  is the orientation contribution of the  $k$ th fiber.

### 1.3 Investigation Tools for Studies of FODs

#### 1.3.1 Traditional Methods

At present, one of the most common methods to obtain three dimensional fiber orientation data involves cutting and polishing the sample down to the locations where FOD are needed. Analysis of the shapes of the elliptical fiber cross sections exposed by physical sectioning is performed as shown in Figure 2. The in-plane orientation angle  $\phi$  is determined from the direction of the major axis of the exposed ellipse, while the out-of-plane angle  $\theta$  is calculated from the ratio of the major to minor axis.

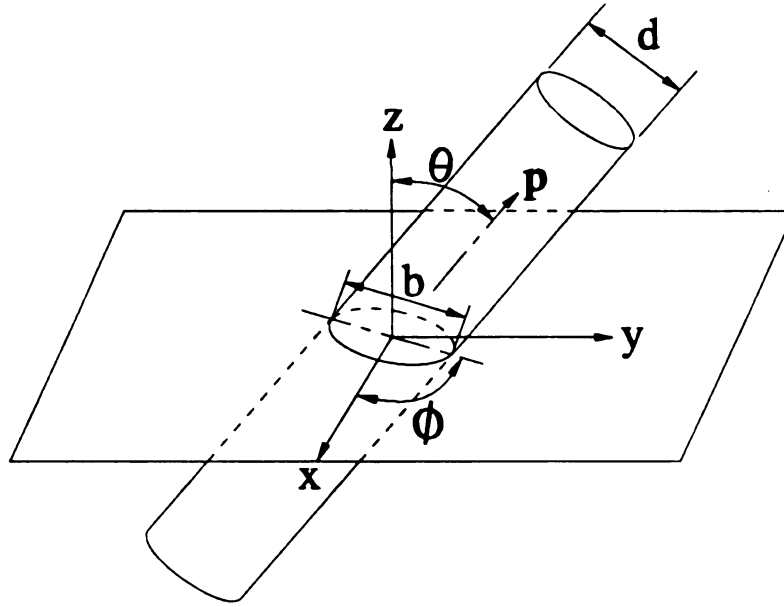


Figure 2. Determination of FODs by Cut/Polish Method.

This method falls into the category of metallographic polishing technique. The disadvantages of this technique are obvious since it is destructive, time consuming, and might introduce ambiguity into the orientation data because fibers with angles  $\theta$  and  $\pi - \theta$  have the same cross sections. Elaborate effort is needed to eliminate this ambiguity using techniques such as optical diffraction or physical etching. The other shortcoming of this method is that it does not provide fiber length information, which is very important for several reasons. For example, fiber-fiber interaction modeling is closely related to the fiber length, the mechanical properties also depend strongly on the length distribution, and the length information can also affect the confidence level calculated for the FOD determinations.

### **1.3.2 Optical Sectioning**

An unique technique has been developed in our laboratory at Michigan State University for the investigation of three dimensional fiber orientation distributions (Wille, 1993). It is nondestructive, capable of providing detailed and complete 3-D information, as well as being accurate and rapid. This technique utilizes optical sectioning, which will be explained in detail in the next section.

## **1.4 Optical Sectioning for SF RTP Research**

### **1.4.1 Basic Concepts of Optical Sectioning**

In our studies, optical imaging is made possible by matching the refractive indices of the matrix material (PMMA) and the glass fiber (BK-10). For most short fiber reinforced thermoplastic composites, the bulk materials usually are opaque or translucent because either one of the components of the composite is opaque, or the interfaces between the fiber and matrix strongly scatter incident light due to mismatched refractive indices. By matching the refractive indices of PMMA and BK-10 ( $n=1.49$ ), we have been able to produce transparent composite samples consistently. A small amount of opaque tracer

fibers (0.2Wt%) is introduced into the mixture to provide statistical representation of the behavior of the glass fibers. An inverted light microscope is used to obtain the image of the tracer fibers. The optical system was modified by introducing a condenser and diffuser to obtain a very narrow depth of field which is approximately the same as the fiber diameter (15 microns). This configuration proved to have minimum information loss and required minimal storage space for the data. In this optical sectioning method only the portion of the sample which intersects the focal plane within the thickness of the depth of field of the optical system is visible. This is what is referred to as **optical sectioning**. The complete 3-D representation of the fiber orientation in the

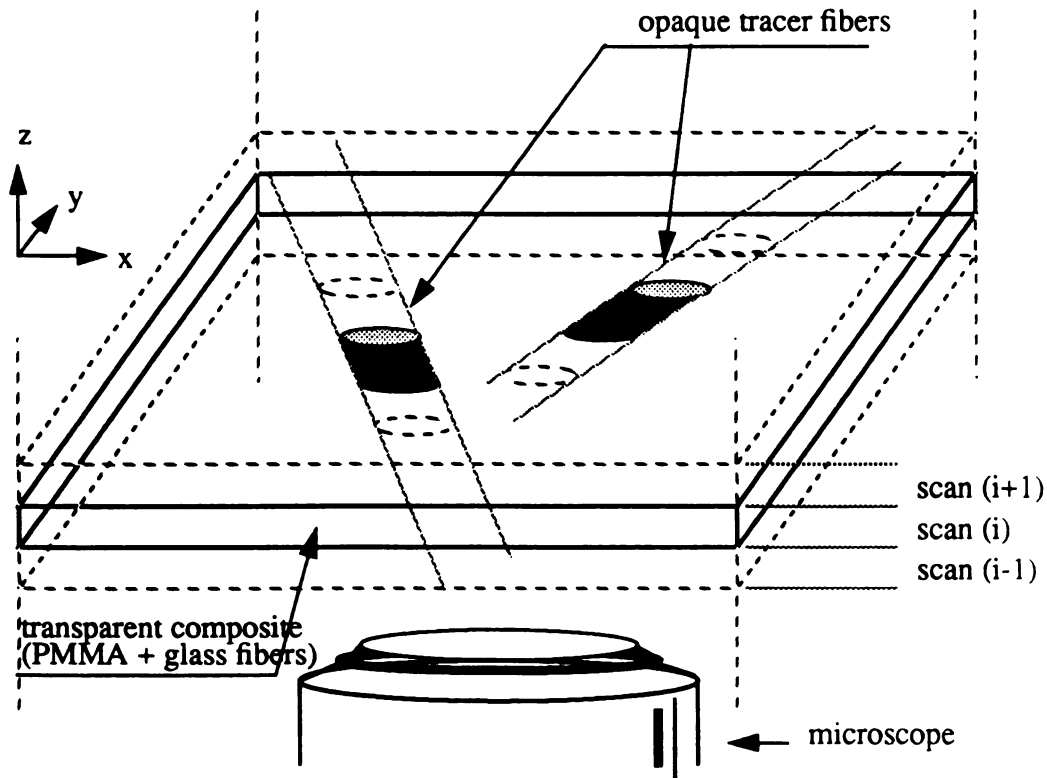


Figure 3. Schematic of Optical Sectioning.

scan cell is obtained by stacking the 2-D images sequentially, as shown in Figure 3. A picture of an actual 2-D image is given in Figure 4. The black segment is the portion of the tracer fiber which intersects the focal plane. The negative of these images are compressed and stored since they require less disk storage space.



Figure 4. A 2-D Image: From Which 3-D Image is Constructed.

#### **1.4.2 Advantages of the Optical Sectioning Method**

Compared with the traditional cut/polish method, the optical sectioning method has proved to be accurate, nondestructive, and rapid. The cut/polish



technique may introduce ambiguity into the fiber orientation data, and requires correction to account for differential probability of fibers with different orientation and length intersecting the polished plane. For the optical sectioning method, the material selections are limited since the specimen have to be transparent. Nevertheless, we have a reasonably wide variety of polymer materials to select from with different refractive indices. The refractive index of the glass can be modified by controlling the addition of chemical compounds, making it possible to apply this technique to other material system that one may be interested in. Table 1 and Table 2 list the refractive indices of most common glass and industrial polymer materials.

**Table 1: Refractive Indices of Glass.**

Glass	Refractive index	Remarks
BK-10 glass	1.49	
Quartz	1.55	
E-Glass	1.56	
C-Glass	1.57	
D-Glass	1.59-1.63	depends on composition

**Table 2: Refractive Indices of Transparent Industrial Polymers and Possible Matches with Glass.**

Material	Refractive Index	Remarks	Glass
Poly(tetrafluoroethylene)	1.35-1.38		
Poly(vinyl fluoride)	1.46		
Poly(butyl acetate)	1.463		
Poly(ethyl acrylate)	1.468		
Poly(methyl acrylate)	1.48		
Poly(methyl methacrylate)	1.49		BK-10
Polypropylene	1.49-1.50		BK-10
Cellulose acetate	1.50		
Polyethylene (Low Density)	1.51	depends on degree of crystallinity	
Polyethylene (High Density)	1.53		
Polyisoprene(Nature Rubber)	1.52		
Polyacrylonitrile	1.52		
Polybutadiene	1.52		
Nylon 11	1.52	depends on degree of crystallinity	
Nylon 6	1.53		
Nylon 6:6	1.53		
Acrylonitrile-butadiene-styrene	1.538		
Poly(vinyl chloride)	1.54		
Styrene acrylonitrile copolymer	1.57		C-Glass
Epoxy Resins	1.57-1.61	depends on composition	C-Glass
Polycarbonate	1.58		
Poly(ethylene terephthalate)	1.58-1.63		D-Glass
Polystyrene	1.590		D-Glass
Polyimide	1.70		

### 1.4.3 Injection Molding Apparatus

Without buying a costly industrial injection molding machine but still retaining the characteristics of the real industrial process, a laboratory scale injection molding apparatus prototype was built (Wille, 1993). It features a simple ram type injector. The sandwich construction of the mold design allows flexibility in changing the geometry of the mold cavity at very low cost. Temperature and velocity measurements are accurate and easily set. Figure 5 is a the schematic of the injection molding apparatus setup.

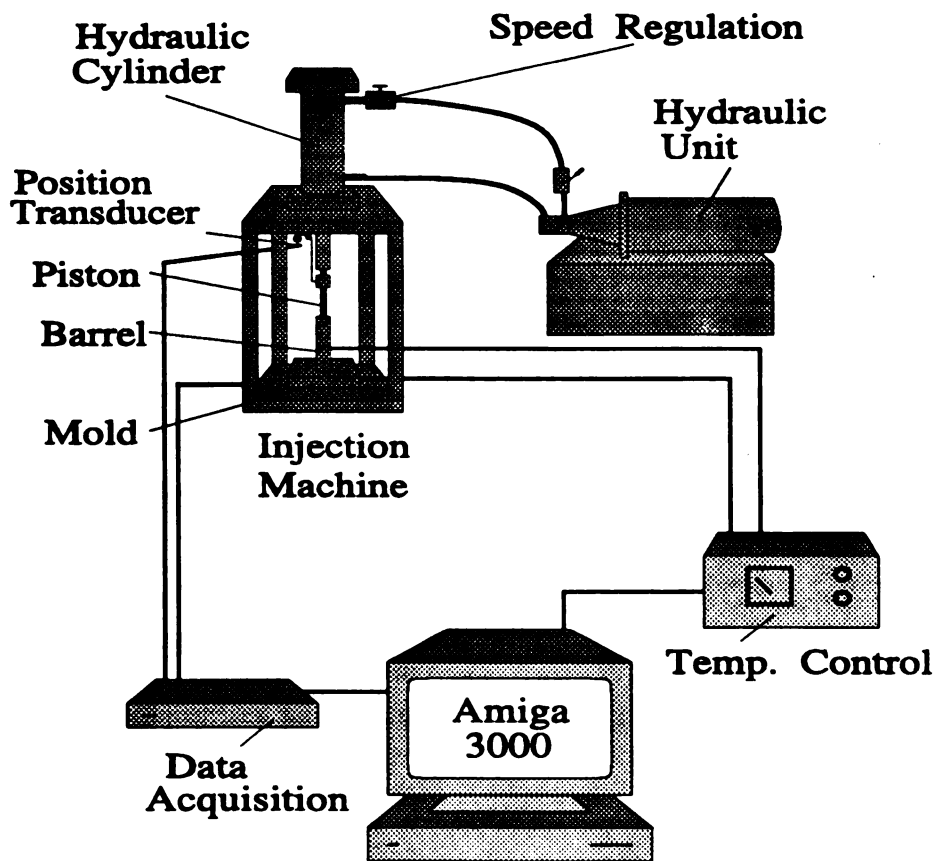


Figure 5. Injection Molding Apparatus.

The operating ranges of processing parameters achieved with this system are relevant to real industrial processing and are listed in Table 3.

**Table 3: Operating Range of Injection Molding Apparatus.**

Parameters	Range
Melt temperature	$20^{\circ}\text{C} \leq T_{melt} \leq 300^{\circ}\text{C}$
Mold temperature	$20^{\circ}\text{C} \leq T_{mold} \leq 120^{\circ}\text{C}$
Injection speed	$100\text{s}^{-1} \leq \dot{\gamma} \leq 1800\text{s}^{-1}; 2.5\text{cm}^3/\text{s} < \dot{v} < 30\text{cm}^3/\text{s}$
Injection/hold pressure	32, 000psi
Mold and gate geometry	Flexible in Mold and Gate Design
Fiber length	$0.1\text{mm} \leq length \leq 3\text{mm}$
Fiber contents	$0 < c < 30\text{ Wt\%}$
Materials	Other Matrix/Fiber Combinations Possible (see Table 1 and 2)

#### 1.4.4 Imaging Apparatus

The optical imaging system includes a Nikon DIAPHOT inverted light-microscope, three programmed servo-motors for automated three-dimensional scanning of specimens, video-camera and frame-grabber for image acquisition and digitizing, and an Amiga-3000 multitasking computer for data processing and storage. The schematic is showed in Figure 6. Since the optical scanning sys-

tem is automated by the computer, it takes much less time to get the same amount of information compared with the cut/polish method (Wille, 1993).

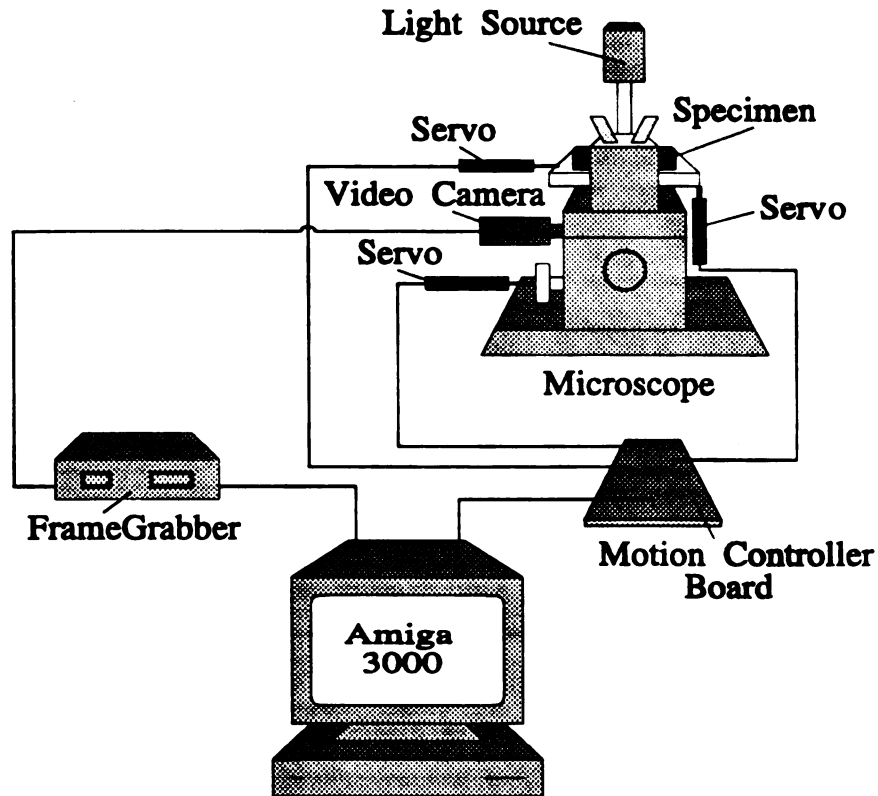


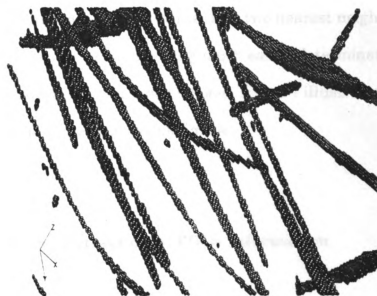
Figure 6. Imaging System.

### 1.4.5 Image Processing Software

#### 1.4.5.1 3-D Thinning

A three dimensional thinning program is used to process the raw image for extraction of fiber orientation distribution information (Wille, 1993). Fiber

materials in the raw images is represented as voxels where each fiber is about several voxels in diameter and tens or hundreds of voxels in length. To deal with the complexity of these structures and to reduce computation time, an



raw image



thinned image

Figure 7. 3-D Thinning.

image skeletonizing algorithm was implemented and used to reduced the raw images to thinned images. A fiber in the raw image is reduced to a thin line segment from which the orientation and length of the original fiber is determined. After thinning each voxel has less than two nearest neighbors, i.e. the connectivity is preserved while providing much easier determination of orientation information from these thinned images. Figure 7 illustrates the effect of 3-D thinning for the three dimensional image.

#### **1.4.5.2 3D-FODAS - Extraction of FODs Information**

After the image is thinned, it needs to be analyzed and the fiber orientation distributions within the image must be described in one way or another. In our studies, two methods have been used for the FODs description. A second order as well as a fourth order tensor description are given since the orientation and length information for each individual fiber are unambiguously known. We also use a direct way to represent the FODs visually in the form of a three-dimensional spherical histogram (Wille, 1993). A subdivided icosahedron (a sphere divided equally into 20 triangular facets) is used to represent the possible orientation of fibers. How many times the triangular facets are subdivided is referred to as the tessellation order. The elevation above the “sea-level” of the sphere represents the accumulation of fiber materials (length) that coincide with the direction  $(\theta, \phi)$  of the corresponding triangu-

lar facets, as illustrated in Figure 8.

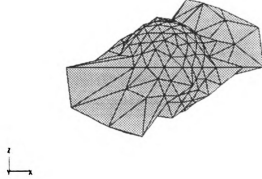


Figure 8. Visualization of FOD by 3D-FODAS.

#### 1.4.5.3 FIBOR - Ellipsoid Visualization

A tensor visualization program is also available which creates graphic representation by projecting the ellipsoid of the second order tensor to the x-y, y-z, and x-z plane (Schoche,1993). An example is shown in Figure 9 for a second order tensor given as follows:

$$\langle a_{ij} \rangle = \begin{bmatrix} 0.700 & 0.000 & 0.100 \\ 0.000 & 0.015 & 0.000 \\ 0.100 & 0.000 & 0.015 \end{bmatrix}$$



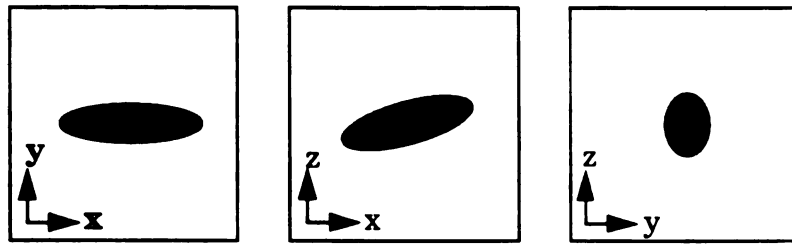


Figure 9. Visualization of Second Order Tensor.

#### 1.4.5.4 PSEUDO - Generation of Images with Specified FODs.

After the image acquisition system had been implemented, a software (PSEUDO) was also developed to provide noise-free images to test how well the image processing program work. The software is capable of producing a simulated image which contains cylindrical fibers that have well defined shapes, lengths and orientations. Fibers with specified length and diameter can be produced.

#### 1.4.6 Some Perspectives for the Development of Optical Sectioning Technique

Having finished setting up the system and many major problems concerning the workability of the optical sectioning technique having been solved, exper-

iments are needed to answer the following questions concerning the usefulness and accuracy of this new measurement tool:

- 1) Are the imaging system and the image processing software capable of producing accurate and consistent results?
- 2) Are the FOD results produced by the optical sectioning comparable to data in the literature which is given by the traditional cut/polish method?
- 3) What are the effects of changing the parameters in the image processing software such as voxel sizes, Tessellation orders? Are their effects significant?
- 4) Among all the possible sources of errors for the FOD measurement, which are those which are the most significant and important?
- 5) To achieve the objective of FOD research for SF RTP design, what are the most important processing parameters that influence the FODs?

The above questions has been carefully considered throughout this project and positive answers and explanations have been acquired and will be shown in the following chapters.

## **Chapter 2**

# **Calibration**

### **2.1 Calibration Using Pseudodata**

A software program called PSEUDO has been developed to create simulated images which contents fibers of desired and known orientation. Since the image is noise free, it can be used to quantify the accuracy of the analysis software and detect any bias (systematic error) introduced by the software.

An ideal 3-D random fiber orientation distribution which contained 81 straight fibers  $600\ \mu m$  long and  $10\ \mu m$  in diameter was created by the PSEUDO Program using the actual voxel sizes ( $1.993 \times 3.367 \times 14.900\ \mu m$ ) used for real images. The pseudo fibers were placed in random locations within the sample volume of  $1077 \times 797 \times 1000\ \mu m$  and oriented uniformly in all directions in 3-D space. For a random fiber orientation distribution, the diagonal elements of the second order tensor are  $1/3$  and all off-diagonal ele-

ments are zero. The simulated image was analyzed and compared with these known values.

## **2.2 Single Fiber Calibration**

Previous tests (Wille and Schoche, 1993) demonstrated that the optical imaging system and the analysis software can measure the fiber length and angle for individual fibers to very high accuracy ( $2^\circ$  error for in-plane and out-of-plane angle measurements and 3% error in length measurement) compared with other available techniques (approximate  $10^\circ$  error in angle measurement and no length information).

To define the uncertainty in our measurements, tests were carried out by measuring the in-plane angles of two carbon fibers and comparing them with the angles measured by the analysis software (Wille, 1993). These tests were repeated by rotating the sample for a total of 90 degrees with 10 degree increments. A maximum error of 2 degrees in fiber angle and 3% in length were found, which are the measurement uncertainty for angle and length for in-plane fibers.

Tests were also done to estimate the uncertainty in measuring out-of-plane

angles. A carbon fiber was placed in the air tilting out of the horizontal plane and was measured using the optical imaging system, it was found that the maximum error for the out-of-plane angles is about 2 degrees and the length measurement was less than 2% in error (Wille, 1993).

### **2.3 Orthogonal Specimen**

Since there is not a standard fiber orientation distribution available to be compared with, the other calibration experiment was carried out by cutting a small volume of dimension 10.3mm x 1.5mm x 1.5mm from the center of one of the samples. A specified volume (1.077mm x 0.797mm x 0.797mm) within this specimen were scanned in four orthogonal directions sequentially. The second, third and fourth scans were made by rotating the specimen 90°, 180°, 270° with respect to the first scan direction, as shown in Figure 10. The four images were thinned, analyzed and rotated mathematically back to the same viewing (reference) direction as the first scan. If certain kinds of systematic errors were present, for example, which could possibly be created by non-uniform voxel sizes, the FODs from these four scans will not be the same.

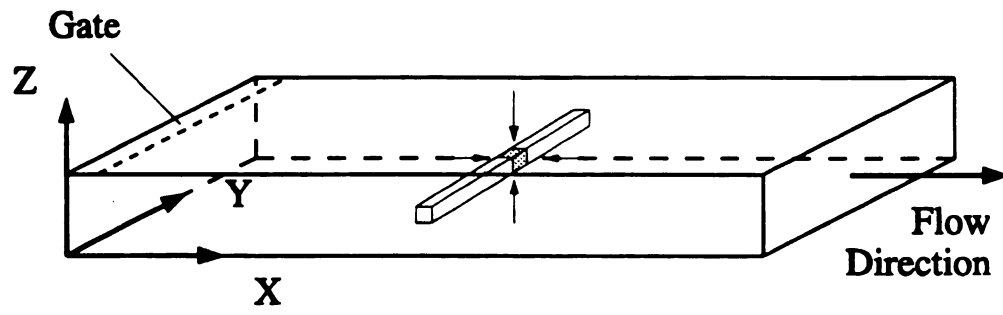


Figure 10. Orthogonal Scans.

## Chapter 3

# Comparison of FODs by Optical Sectioning and Cut/Polish Method

To verify that the optical sectioning technique provides results that are comparable to the results given by the traditional method, samples were investigated using optical scanning and then subjected to physical cutting and polishing followed by surface ellipse analysis of the same volumes. The data were taken from the middle of the samples ( $x/L \sim 0.5$ ) as shown schematically in Figure 11 and comparisons were made for two samples, sample no8 and

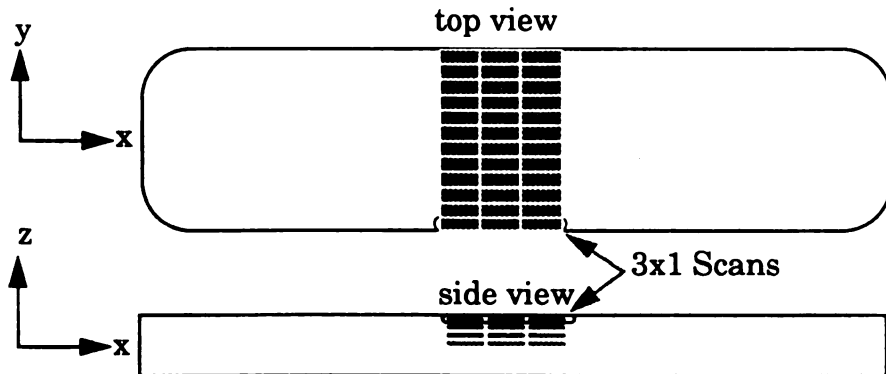


Figure 11. Scan Locations for Optical Sectioning and Cut/Polish.

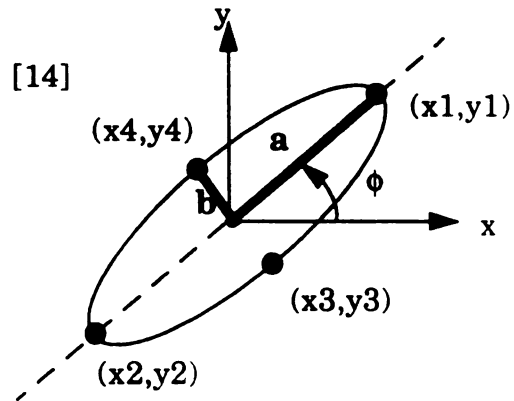
sample ob7.

3x1 scans were made to obtain a single measurement. A 1x 1 scan cell corresponds to the minimum imaging area in x-y plane defined by the optical system which is  $1077 \times 797 \mu m$  and the z dimension ( $150 \mu m$ ) is obtained by putting together 10 slices of 2D images  $15 \mu m$  thick each. Comparisons were made at four different through-thickness (z) locations and twelve transverse (y) locations.

In this comparison experiment, optical sectioning was carried out before the samples were polished down to various through-thickness locations. The shapes of the ellipses on the cutting plane were analyzed. The rotation angles  $\phi$  were calculated by measuring the angle between the major axis of the ellipse and the x-axis (flow direction). The elevation angles  $\theta$  were obtained by comparing the ratio of the major axis **a** to the minor axis **b** of the ellipses:

$$\phi = \text{atan}\left(\frac{y_2 - y_1}{x_2 - x_1}\right) \quad [13]$$

$$\theta = \text{acos}\left(\frac{\sqrt{(y_4 - y_3)^2 + (x_4 - x_3)^2}}{\sqrt{(y_2 - y_1)^2 + (x_2 - x_1)^2}}\right) \quad [14]$$





## **Chapter 4**

# **Image Processing**

### **4.1 Image “Crushing” to Remove Fiber Clumps**

For given sharp and clean fiber images, the 3D thinning software works well to reduce the raw images to thin line segments. However, sometime the image quality is not so good and contains non fiber information, such as shadows created by abnormal fiber aggregation, dirt and voids present in the specimens, these are referred to as “fiber clumps”. The shadows are most likely to occur for images taken deep inside the specimens since in this region the optical path is partially blocked by the opaque fibers sitting in between the focal plane and the optical lens. The thinning program processed the fiber clumps down to hairy structures which significantly influenced the FOD results, especially for the core layer. The magnitude of  $\langle a_{11} \rangle$  was reduced slightly, but the magnitude of  $\langle a_{33} \rangle$  was increased from the typical value of 0.1~0.2 to 0.3~0.4. Based on the original program written by Jeff Wille, an image preprocessing

algorithm was implemented to deal with the problem. This preprocessor divides the whole image plane into small square cells of dimension about 50 x 50 microns and checks the percentage of the voxels set in each cell. If it is over 40%, a square is defined which has the same center but twice the size of the original cell, voxels inside it are erased, as showed in Figure 12. The dimen-

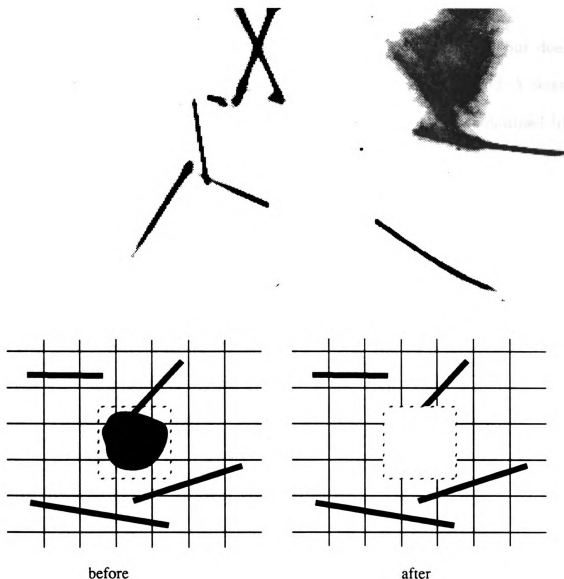


Figure 12. Sample Image with Fiber Clumps and the Schematic of the Image Preprocessing for Fiber Clumps Removal.

sion of the cells was chosen in such a way that it was comparable to the size of the fiber clumps but considerably larger than the fiber diameter. The 40% criteria takes into account the possibility that two fibers could be in the same cell even for good images and these should not be erased. The possibility of having more than three fibers inside a same cell is so low that it is negligible.

To verify that the algorithm does not affect good quality images but does remove the fiber clumps if they exist, two test cases were studied. A clean image containing a random fiber distribution and real images obtained by through-thickness scanning were both used for the tests.

The random fiber orientation distribution created by the PSEUDO program were used to check how much the algorithm would affect the FOD results of a clean image. Actual images obtained by optical sectioning which contained 3 x 3 scans from the surface to the midplane at  $x/L=0.5$  were used to test the effects of the algorithm to images containing fiber clumps.

#### **4.2 Influence of Non-Uniform Voxel Sizes on FODs.**

A possible source of systematic error involves the utilization of different voxel sizes in the x, y, and z directions to represent fiber materials. The three dimensional images are obtained by linking two dimensional images together

sequentially. The third dimension is added knowing the scanning step size in the sectioning (z) direction. The voxel sizes in the x, y, and z direction are 3.367, 1.993, and 14.900  $\mu m$  respectively for the optical imaging system. It is of interest to determine whether the nonuniformity in voxel size will affect the quantitative results for FODs significantly, noting that even though the thinning takes place uniformly in all directions, the non-uniform voxel sizes could possibly create bias FOD results.

Analysis was done using the sample for the orthogonal scans and two step sizes were used in the sectioning direction to obtain two different voxel sizes, i.e., 14.900 and 7.450  $\mu m$ .

## **Chapter 5**

# **Error Estimates and Analyses**

### **5.1 Motivation**

Error estimates and analyses are very critical in this study in order to prove that the optical sectioning method is accurate while possessing other advantages over traditional techniques. Any measurement tool should not only have the capability to produce experimental data, but also should provide confidence limits for the information obtained from it. Uncertainty estimate analysis is important relative to the improvement of system accuracy by identifying the sources of errors and the sensitivity of overall uncertainty to various parameters. It is also important to define the confidence level for those data that have been produced such that quantitative comparison of FODs of the SF RTP fabricated under different processing conditions can be made. Thus conclusions with quantitative confidence limits can be derived.

## **5.2 Possible Sources of Errors**

Errors and uncertainties in fiber orientation measurement can be classified into three categories: systematic, measurement and sampling errors. Systematic error is any nonrandom difference between measured and actual quantities which can not be eliminated by using larger sample sizes or more repetitions. Measurement error is related to the random variation expected when a measurement is repeated on the same sample and which can not be improved by using larger sample sizes. Sampling error denotes the variation among measurements expected for different samples from the same population.

### **Systematic errors:**

This kind of error stems from the inaccuracy or bias of the measurement tools and methods which creates persistent differences between the measured values and the actual values. These kinds of errors can only be eliminated by using better measurement equipment. They may be identified by comparing measurement results using other techniques. In our study, the following factors might be most important:

- alignment of sample on the optical stage

comments: several degrees of systematic error can be introduced

into the angle measurement if it isn't done correctly.

Make sure sample is free of flash and attached to the stage correctly.

- calibration of the optical system including alignment, magnification, etc.

comments: check occasionally and make sure there are no loose parts in the optical path.

- possible bias created by imaging system and analysis software

comments: the thinning program could shorten the fiber length by the amount of one fiber diameter, which doesn't noticeably influence the results. The non-uniform voxel sizes could also create bias FOD results, tests done showed no significant influence.

### **Measurement errors:**

Uncertainty in the quantities being measured, condition of the measurement tool, operator effect and other factors all contribute to the measurement errors. Care must be taken to minimize the possible errors.

- resolution limit of the image digitizing

comments: this imposes an uncertainty of angle measurement of

about 4.3 degree (based on  $\Delta d(z\text{-resolution}) = 14.9\mu m$ ,

$L = 200\mu m$ ,  $\frac{\Delta d \times 180^\circ}{\Delta L \times \pi} \cong 4.3^\circ$ ). This is comparable to the

discrete angle interval used to describe FODs (for tessellation order 4, the interval is 5 degree).

- change and fluctuation of light intensity

comments: light intensity has a lot to do with the FOD results since it not only changes the apparent fiber length but it also influences the results related to the through-thickness direction because the image of fibers tends to stay on the screen for a longer time if light intensity is higher. It should be high enough to make sure that all of the individual fibers are connected to get the correct length information but low enough so as not to exaggerate the z dimension. Careful adjustment of light intensity is the key point to reduce this error to a minimum, and a better power supply or stabilizer could be used to eliminate the intensity fluctuation.

**Sampling errors:**

Sampling error describes the inherent variation within the measured quantity or quantities. Measurements should be made repeatedly for samples produced under the same condition so that the measurement can be treated as random independent quantities. In the investigation of fiber orientation distribution, it means we need to measure the orientation of a single fiber from each individual sample of a large enough population. It is nearly impossible to



produce and collect FOD information from such a large sample size. To deal with this problem, we usually assume that fibers which are about one fiber length apart can be considered as independent and sampling can be done within these locally homogeneous regions. This assumption is a true approximation if fiber-fiber interaction is a short range phenomenon.

### **5.3 Confidence Limit on FODs**

#### **- Standard Error of Tensor Components**

It has been widely accepted that processing influences the FODs in SF RTP. The confidence limits on the FODs are as important as the FODs themselves, especially when comparisons are to be made to determine if different processing conditions produce different FOD results.

Fiber orientation distributions are approximated by second order tensors which consist of nine tensor components, within which only five of these nine components are independent. The geometrical analogy of the second order tensor is an ellipsoid. These five parameters are needed to give a full description of the ellipsoid, which includes the shape (aspect ratio) and orientation.

From the definition of the tensor components, for example, for  $\langle a_{11} \rangle$ :

$$\langle a_{11} \rangle = \langle \sin^2 \theta \cos^2 \phi \rangle = \frac{\sum_{i=1}^N l_i \cdot a_{11}^i}{\sum_{i=1}^N l_i} \quad [15]$$

(where  $l_i$ ,  $a_{11}^i$  are the length, the tensor component for the  $i$ th fiber and  $N$  is the total number of fibers). It can be seen that it is a weighted average of all the fibers in the sampling population. We would like to know how accurate these parameters are for certain fiber orientation distributions. Noting that  $\langle a_{11} \rangle$  is one of the five parameters (tensor components) to describe the FODs, the standard deviation of the mean  $\langle a_{11} \rangle$  is an appropriate measure of the uncertainty of  $\langle a_{11} \rangle$ . Since  $\langle a_{11} \rangle$  is a length-weighted average of all the  $a_{11}$  for each individual fiber within the scan cell, the standard deviation of the mean (standard error) which gives the accuracy of  $\langle a_{11} \rangle$  at 95% confidence level can be calculated as follows (Advani and Tucker, 1992):

$$SE(a_{11}) = 2.0 \sqrt{\left( \frac{\sum_{i=1}^N l_i \cdot (a_{11}^i - \langle a_{11} \rangle)^2}{\sum_{i=1}^N l_i} \right) \cdot \left( \frac{\sum_{i=1}^N l_i^2}{\left( \sum_{i=1}^N l_i \right)^2} \right)} \equiv \frac{2.0 \cdot SD(a_{11})}{\sqrt{N}} \quad [16]$$

where  $SD(a_{11})$  is the standard deviation of  $(a_{11})$  and  $N$  is the total number of fibers sampled. For a given homogeneous population,  $SD(a_{11})$  describe the dispersion of the fiber orientation and will be the same for any subdomains (partitions) within the total population, provided these subdomains have enough fibers to give statistical meanings. An empirical relation can be derived

between the magnitude of  $SE(a_{11})$  and number of fibers  $N$  if the range of  $SD(a_{11})$  is available. Figure 13 demonstrates typical ranges for  $SD(a_{11})$  for the shell and core layers, as well as the  $SE(a_{11}) \sim N$  relation deduced from them.

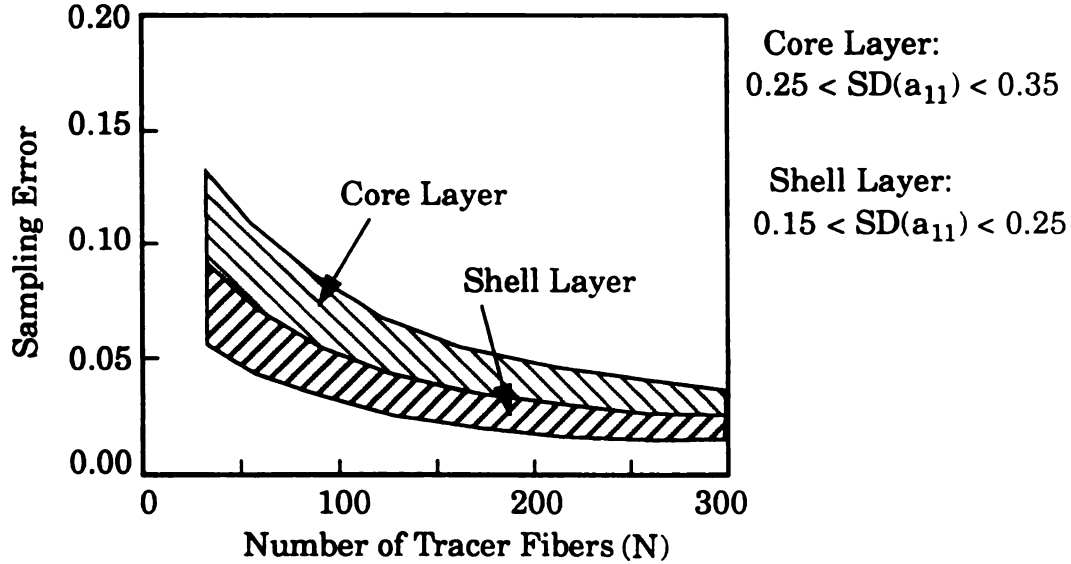


Figure 13. Sampling Error versus Number of Tracer Fibers.

As we will see in the next section, the measurement errors (usually about 0.01 to 0.02) is consistently smaller than the sampling errors (standard errors, 0.02 ~ 0.13). The biggest error, i.e., the standard error will be reported in this study, except when pointed out specifically. It is also believed that the systematic error is smaller than the measurement errors since no significant biased result has been detected.

## 5.4 Estimates of Measurement Error

Comparison between the experimental uncertainty for the second order tensor components and the estimates of the error analysis is necessary to determine which measurement errors are most important to the overall uncertainty so that they can be identified and improved. An uncertainty estimate for the measurement errors was performed. Having acquired an explicit expression for the tensor components in terms of the measurement variables (angle, length), a sensitivity study was carried out to determine which measurement uncertainty contributes the most to the total variation. An estimate of the total uncertainty is also defined. For a given relation:

$$\Delta f(x_1, x_2, \dots, x_n) = \sqrt{\left(\frac{\partial f}{\partial x_1}\right)^2 (\Delta x_1)^2 + \left(\frac{\partial f}{\partial x_2}\right)^2 (\Delta x_2)^2 + \dots + \left(\frac{\partial f}{\partial x_n}\right)^2 (\Delta x_n)^2} \quad [17]$$

The following gives the calculation for the estimated measurement error for tensor component  $\langle a_{11} \rangle$ :

From the definition of  $\langle a_{11} \rangle$ :

$$\langle a_{11} \rangle = \frac{\sum_i l_i \cdot (\sin \theta)^2 \cdot (\cos \phi)^2}{\sum_i l_i} \quad [18]$$

the sensitivity coefficients can be found as follows:

$$\frac{\partial}{\partial l_i} \langle a_{11} \rangle = (\sin \theta)^2 \cdot (\cos \phi)^2 \cdot \left( \frac{1}{\sum_i l_i} + \frac{-l_i}{\left( \sum_i l_i \right)^2} \right) \equiv \frac{(\sin \theta)^2 \cdot (\cos \phi)^2}{\sum_i l_i} \quad [19]$$

$$\frac{\partial}{\partial \theta_i} \langle a_{11} \rangle = \frac{2l_i \cdot \sin \theta_i \cos \theta_i (\cos \phi_i)^2}{\sum_i l_i} \quad [20]$$

$$\frac{\partial}{\partial \phi_i} \langle a_{11} \rangle = \frac{2l_i \cdot (\sin \theta_i)^2 \sin \phi_i \cos \phi_i}{\sum_i l_i} \quad [21]$$

and finally,

$$\Delta \langle a_{11} \rangle = \sqrt{\sum_i \left( \frac{\partial}{\partial l_i} \langle a_{11} \rangle \right)^2 (\Delta l)^2 + \sum_i \left( \frac{\partial}{\partial \theta_i} \langle a_{11} \rangle \right)^2 (\Delta \theta)^2 + \sum_i \left( \frac{\partial}{\partial \phi_i} \langle a_{11} \rangle \right)^2 (\Delta \phi)^2} \quad [22]$$

3 x 1 scans (each 1077 x 797 x 150  $\mu m$ ) were repeated ten times for both core and shell layers respectively, as illustrated in Figure 14. The means and uncertainty of the tensor components were calculated. The error estimates were performed knowing the orientation and length information of the fibers in these images.

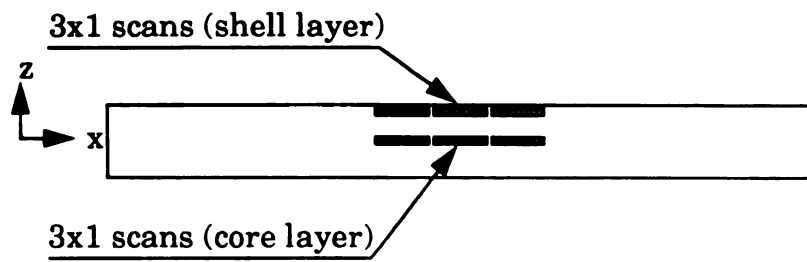


Figure 14. 3 x 1 Repeated Scans in the Shell and Core Layers.

## **Chapter 6**

# **Influence of Processing Parameters on FODs**

### **6.1 Injection Molding Process**

Injection molding is a very complicated process. Basically it includes: (1) the melting of the filled or unfilled polymeric material; (2) mold filling during which the pressurized melts flow into the mold cavity; (3) the packing and (4) cooling. Theories of fluid mechanics, polymer rheology, and heater transfer are all needed to explore the physical nature of this process.

Substantial efforts have been put into the investigation of the mold filling process for short fiber reinforced thermoplastics, both in theory and experiment by different research groups. Several commercial versions of simulation software are already available. Tucker (1991) and Wang (1993) give very nice reviews about these work in this area.

For example, during the filling process of a simple mold geometry such as a rectangular slit, heat transfer occurs from the hot melt to the cold mold through the cavity wall and produces a through-thickness nonuniform temperature distribution. Under this non-isothermal condition the temperature field during injection molding is characterized by thin cold boundary layers near the walls and a hot core region away from the walls. The significance of the influence of the solid boundary layers on the flow field and eventually the FODs depends on the ratio of the solid layer thickness and the height of the cavity. The effect of the solidified layers upon the through-thickness velocity profile is shown in Figure 15:

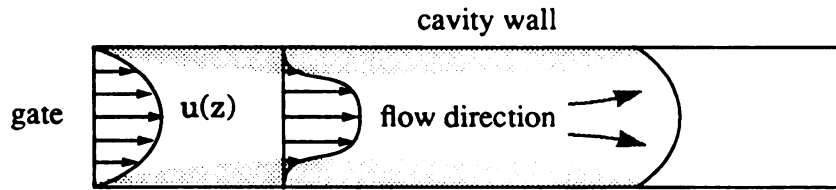


Figure 15. Formation of Solid Boundary Layer and Velocity Profile.

The heat transfer process can be characterized by several non-dimensional numbers (Tucker 1991):

$$Gz = \frac{4b^2}{\alpha t_{fill}} = \frac{\text{heat conduction time}}{\text{mold filling time}}; (\text{Graetz Number})$$

$$Br = \frac{\eta V^2}{k(T_{melt} - T_{mold})} = \frac{\text{heat dissipation rate}}{\text{heat conduction rate}}; (\text{Brinkman Number})$$



$$Pn = \zeta (T_{melt} - T_{mold}) = \frac{\text{Temp. difference between mold and fluid}}{\text{Temp. difference to change viscosity}}; \text{ (Pearson Number)}$$

The thickness of the solid boundary layer is approximately given as

$$\frac{b}{\sqrt{Gz}} = \sqrt{\alpha t_{fill}}, \text{ which indicates that a high injection rate produces thin solid}$$

boundary layers and a slow injection rate leads to a thick boundary layer. Due to the highly viscous nature of polymer melts there is significant local energy build-up created by shear heating and if this energy is not dissipated fast enough through conduction or convection, a temperature increase will occur which will change the viscosity of the melt and eventually the velocity profile. This effect can not be neglected since the Brinkman number is around 10 for a typical injection molding process. The Pearson number is always large ( $\sim 10$ ) (for  $\zeta \sim 1/20^\circ\text{C}$ ), indicating that a solid boundary layer is constantly formed on the mold wall.

## 6.2 Processing Parameter Influences on the FODs

One of the characteristics of fiber reinforced, injection molded parts is that the fiber orientation distribution displays different behaviors at different locations through the thickness. This variation has been called the layered structure. Fibers near the cavity wall experience high shearing and tend to be aligned along the flow direction which creates a highly aligned shell layer.

Fibers near the centerline of the cavity experience no shear and carry the initial orientation state (assumed to be random) near the gate into the mold cavity, leading to the somewhat random core region.

There are a number of processing parameters which could influence the FODs, however they are not equally important. To identify the most significant ones is a very important process as it is linked directly to optimal design for short fiber reinforced thermoplastic parts. The process variables are listed below and their relative importance are also discussed.

### **Injection Speed (volume flow rate)**

Since the differential equations for the second order tensor components contain only the first derivative with respect to length and time, this means that the FODs depend solely on the total (shear or extension) deformation but not on the rate of deformation (shear or extension rate). Thus FODs produced by different injection speeds will be the same under isothermal conditions. However, low injection speed leads to a thick solid boundary layer near the wall which creates a constrained flow path favoring higher fiber alignment along the flow direction and producing a thick shell layer and a thin core layer. This phenomenon is most important when the thickness of the solid boundary layer is not negligible compared with the thickness of the cavity. Another effect that will make the results deviate from the isothermal

prediction is the shear thinning effect which relates to the fact that melt viscosity is shear rate dependent, a common feature observed for most polymer materials.

### **Melt Temperature**

The influence of the melt temperature on FODs mainly comes from the temperature dependence of the power law index  $n$  ( $0 < n < 1$ ,  $\eta = m\dot{\gamma}^{n-1}$ ). For Newtonian fluids  $n$  equals one. The lower the melt temperature, the closer  $n$  approaches zero, i.e., the non-Newtonian fluid behavior, which corresponds to a blunt velocity profile and a thick core layer. For real industrial processes, the operating temperature range is limited to about 50 degrees for most polymer materials since high melt temperature tends to degrade the material and low temperature requires high processing pressure. The change of  $n$  in this temperature range is small and it usually won't produce significant changes of the FODs. For example,  $n$  varies only from 0.19 to 0.27 for a melt temperature change of 40 degrees (PMMA).

### **Mold Temperature**

Usually the mold temperature is kept low to reduce cycle time in actual industrial processes. For most materials the mold temperature is much lower than the polymer glass transition temperature and a solid boundary layer will be formed. This phenomenon is characterized by a large

Pearson number ( $\sim 10$ ) in the injection molding process (Bay and Tucker, 1991). Changing the mold temperature usually has little effect on the velocity profile and the FODs.

### **Material effects**

It was found that FODs were quite different for samples made using the same kind of materials but different grades (molecular weight). For PMMA of low molecular weight (Dupont Acrylic 2010) which would be expected to exhibit more Newtonian-like behavior, the shell layer was found to be thicker than those samples made using PMMA of higher molecular weight (Kodak). Simulations were performed to explore the difference in FOD results from samples produced using different PMMA.

## Chapter 7

# Results and Discussions

### 7.1 Calibrations

#### 7.1.1 Pseudo Data Calibration

A random fiber distribution created by PSEUDO was processed using the image processing software. The result given by the analysis software is showed as below:

$$[a_{ij}] = \begin{bmatrix} 0.3373 & -0.0014 & -0.0005 \\ -0.0014 & 0.3365 & -0.0012 \\ -0.0005 & -0.0012 & 0.3265 \end{bmatrix} ,$$

result given by analysis software

$$[a_{ij}] = \begin{bmatrix} 0.3333 & 0.0000 & 0.0000 \\ 0.0000 & 0.3333 & 0.0000 \\ 0.0000 & 0.0000 & 0.3333 \end{bmatrix}$$

actual values for  $a_{ij}$

The ideal random distribution has a magnitude of 1/3 for the diagonal elements and zero for all off-diagonal elements for the second order tensor. The actual result showed that the error introduced by the imaging and analysis

was less than 2% for the second order tensor components and the average measured length was 576  $\mu\text{m}$  which was a 4% error.

### **7.1.2 Results from Orthogonal Scans**

Bias in the FOD results may be introduced due to the fact that the voxel used to represent the digitized image has different dimensions in the x, y and z directions. If the imaging system and the image processing software are accurate, the four images obtained from the orthogonal scans and the fiber orientation information extracted from them should be exactly the same. Figure 16 demonstrates the result from these scans. Note that while the details of the FODs are not identical in each view, the basic shape and orientation are similar.

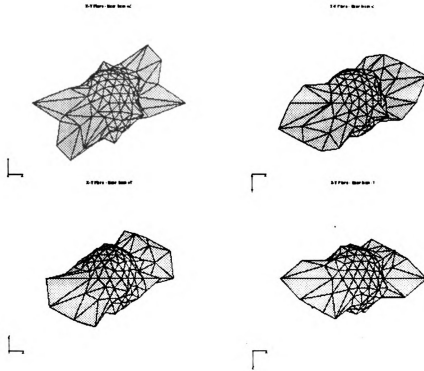


Figure 16. Visualization of Result from the Four Orthogonal Scans.

Table 4 shows the 2nd order tensor components for these four scans (after being rotated back to the same reference orientation) as well as the components of the unit vectors  $e_{major}$  corresponding to the directions of the major axes of the ellipsoids which represent the most populated fiber direction.

**Table 4: Tensor Components and Unit Vectors of Major Axes of the Ellipsoids.  
(Tessellation Order 2)**

	$a_{ij}$			$e_{major}$
scan 1	0.4730	-0.1402	0.2800	0.7253
		0.1985	-0.1662	-0.3505
	sym		0.3284	0.5926
scan 2	0.4370	-0.0787	0.3062	0.6910
		0.1514	-0.1321	-0.2352
	sym		0.4116	0.6835
scan 3	0.4243	-0.1423	0.2697	0.6801
		0.2210	-0.1705	-0.3828
	sym		0.3547	0.6253
scan 4	0.4096	-0.1222	0.2536	0.6420
		0.1767	-0.1794	-0.3526
	sym		0.4137	0.6809

If these four scans are very similar, the directions of the major axes should coincide very closely with each other. The angles between any two of the four unit vectors and the difference from the average direction are summarized in Table 5.



**Table 5: Difference in Directions Between Individual Scans and from the Mean.**

$$\Delta_{ij} = \text{acos}\left(\vec{e}_{major}^i \cdot \vec{e}_{major}^j\right)$$

Angles (in degrees) $\Delta_{ij} = \text{acos}\left(\vec{e}_{major}^i \cdot \vec{e}_{major}^j\right)$	scan1	scan2	scan3	scan4
scan1		8.64	3.62	6.91
scan2			9.11	7.27
scan3				4.16
scan4				
$\overline{\Delta}_i = \text{acos}\left(\vec{e}_{major}^i \cdot \overrightarrow{e_{major}}\right)$	5.82	7.27	5.33	5.43

$\vec{e}_{major}^i$  represents the direction of the major axis from the individual scan and  $\overrightarrow{e_{major}}$  is the average direction.  $\Delta_{ij}$  is the angle difference of the major axes in degrees between any two of the four scans, and  $\overline{\Delta}_i$  is the angle difference of individual scan and the average. It can be seen from the above results that the difference between the individual measurements and the average is approximately 5 to 7 degrees, which agreed with the uncertainty in angle measurement (section 5.2).

Analysis also showed that using higher tessellation order (>2) did not significantly affect the accuracy of the tensor components. Nevertheless, higher tessellation order should be used to obtained accurate length information for

individual fibers since the higher the tessellation order (angular resolution), the less the chance that several fibers will be put into the same “bin” of the subdivided icosahedron.

## 7.2 Comparisons of FOD Results Obtained from the Optical Sectioning and Cut/Polish Method

Figure 18 and Figure 19 are comparisons of the FOD results determined by the two methods within which the lateral (cross flow direction) FOD variations for different through-thickness locations are shown.

Each data point is the average of results from three adjacent scan cells obtained by the 3 x 1 scans in the flow (x) direction. The error bar represents the variation (standard deviation) of  $\langle a_{11} \rangle$  or  $\langle a_{33} \rangle$  within these three cells.

Also presented in Figure 18 and 19 is the significance level of differences between the tensor components obtained from the two methods. The statistical significance (p value) of the difference between tensor components was calculated from the mean and standard deviation of the measurements. The t statistic of the difference between the means was calculated using

$$t(\bar{x}_2 - \bar{x}_1) = \frac{\bar{x}_2 - \bar{x}_1}{\sqrt{S^2_p \left( \frac{1}{n_1} + \frac{1}{n_2} \right)}} \quad [23]$$

$$S_p^2 = \frac{(n_1 - 1) S_1^2 + (n_2 - 1) S_2^2}{(n_1 - 1) + (n_2 - 1)} \quad [24]$$

The t-distribution can be calculated as:

$$F(t) = \int_{-\infty}^t \frac{\Gamma\left(\frac{n+1}{2}\right)}{\sqrt{n\pi}\Gamma\left(\frac{n}{2}\right)} \left(1 + \left(\frac{x}{2}\right)^2\right)^{-\frac{n+1}{2}} dx \quad [25]$$

where the n is the number of degrees of freedom  $n=n_1+n_2-2$ .

The typical shape of the t-distribution is illustrated as follow:

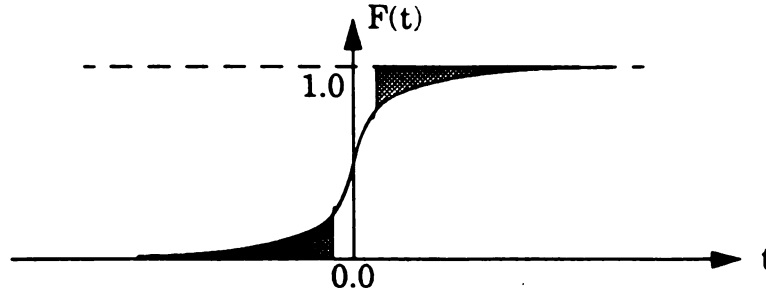


Figure 17. t-Distribution for  $n=4$ .

The p-statistic ( $0 < p < 1$ ) is the shaded area in Figure 17 and it represents the possibility of observing the difference of the means from the two populations greater than the difference of the two means of the known distributions, if the experiments were repeated under the same conditions. The magnitude of p can be affected from the two populations being compared basically in two ways: first, the difference of the means, second, the spread of the distributions. The more the means deviate from each other, or the smaller the standard deviation of the distributions, the smaller p will be, the more distinct of

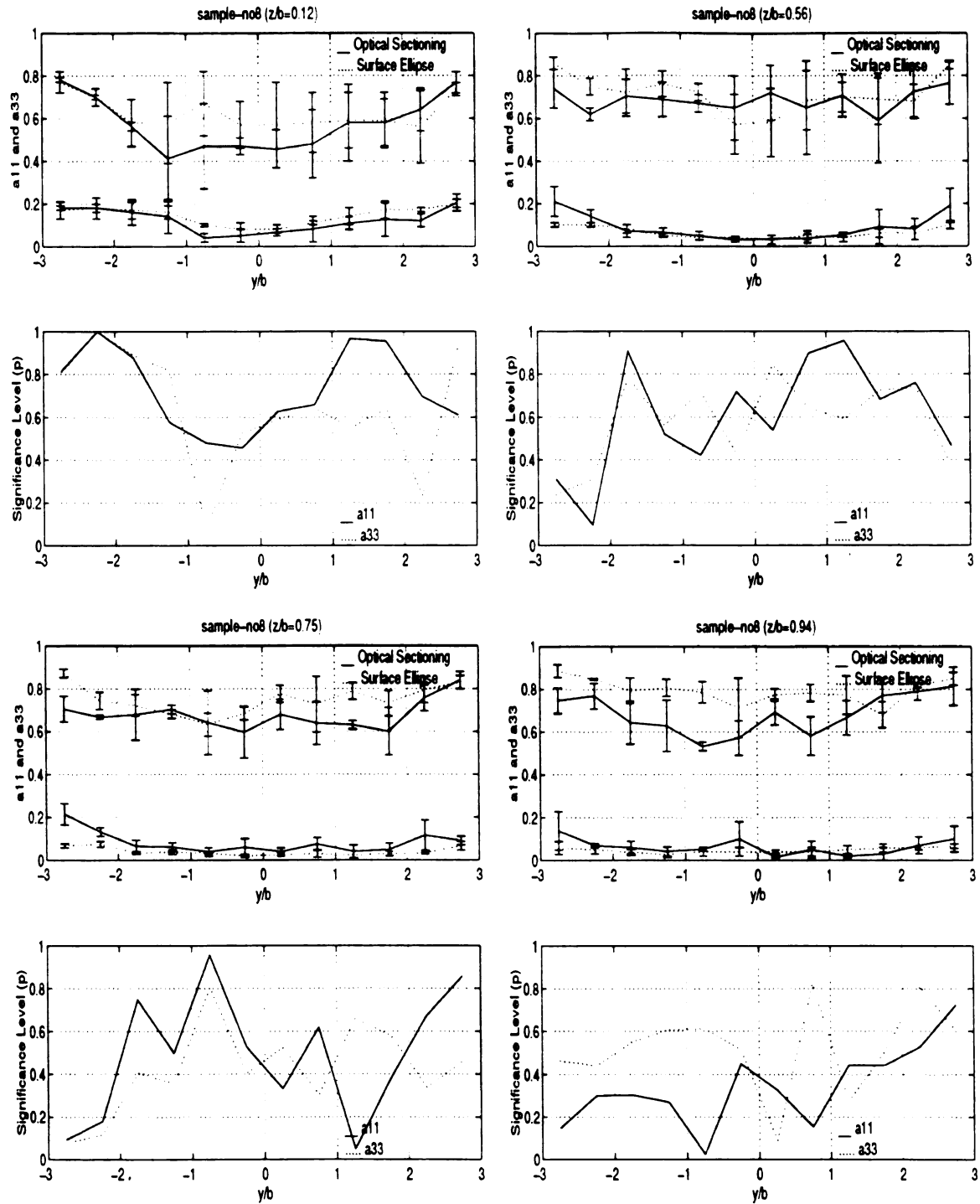


Figure 18. Comparison of  $a_{11}$  and  $a_{33}$  Given by Optical Sectioning and Cut/Polish Method and the Corresponding Significance Level of Difference (Sample no8).

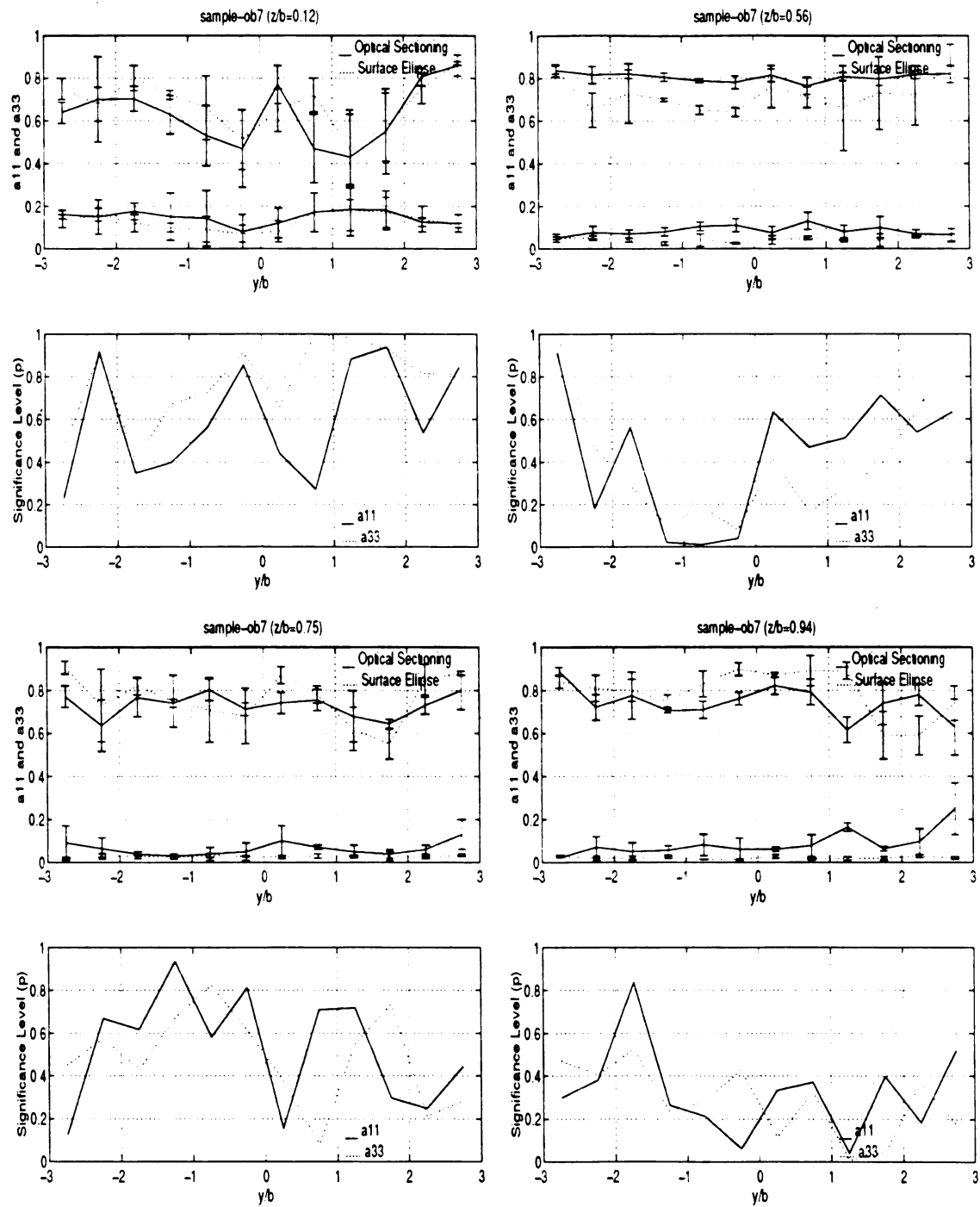


Figure 19. Comparison of  $a_{11}$  and  $a_{33}$  Given by Optical Sectioning and Cut/Polish Method and the Corresponding Significance Level of Difference (Sample ob7).

the difference will be for the two distributions.

The above comparison suggests that the optical sectioning method is capable of producing information similar to FODs obtained by the surface ellipse method. The significant level  $p$  suggested that even though results given by these two methods didn't agree for every points, the overall picture indicated there was no significant difference. The experiment also showed that the optical sectioning is about five times faster than the traditional cut/polish method.

## **7.3 Imaging Processing**

### **7.3.1 Fiber Clumps “Crushing”**

An image processing algorithm was implemented to remove fiber clumps present in the actual images. Tests were performed to define how well this algorithm works and the results showed that it didn't affect clean images (free of fiber clumps) but did remove the clumps when they were present (results shown below). This approach will shorten the fibers near the clumps, but due to the fact that there are only a few clumps in the images, the total extent of shortening of real fiber lengths in the sampled population is insignificant. The following is a comparison of tensor components with and without the preprocessor for a clean image created by the Pseudo program and it shows the ten-

second order tensor components are changed by less than 2%.

$$[a_{ij}] = \begin{bmatrix} 0.3373 & -0.0014 & -0.0005 \\ -0.0014 & 0.3365 & -0.0012 \\ -0.0005 & -0.0012 & 0.3265 \end{bmatrix}; \quad [a_{ij}] = \begin{bmatrix} 0.3384 & -0.0015 & -0.0014 \\ -0.0015 & 0.3391 & -0.0002 \\ -0.0014 & -0.0002 & 0.3225 \end{bmatrix}$$

(a) **without preprocessor**                      (b) **with preprocessor**

The test using actual images showed that for poor images the effect of correcting for fiber clumps is obvious for images with fiber clumps, as shown in Figure 20, which shows reduced  $\langle a_{33} \rangle$  component and slightly increased  $\langle a_{11} \rangle$  component. The preprocessing did not affect the FOD results at all where the image quality was good, for example the shell layer, because it is here where the through-thickness scans start and images are usually sharp and clean. However, when scannings go deeper down toward the core region, fiber clumps are likely to occur, it was found that  $\langle a_{33} \rangle$  in the core layer could be reduced down by approximately 50% by the image preprocessor even though the change in  $\langle a_{11} \rangle$  is not that significant. It is obvious that how much change caused by the image preprocessing to the second order tensor components depends on the image quality.

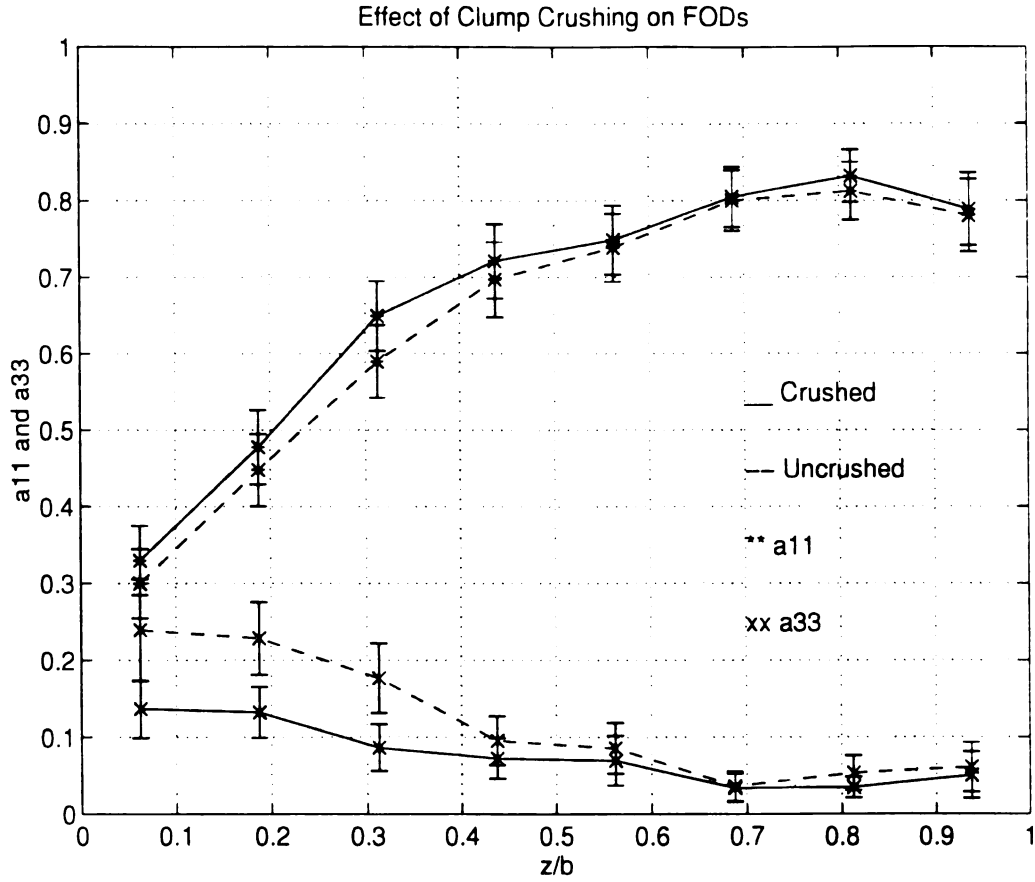


Figure 20. Effect of the Preprocessor for Real Images with Fiber Clumps.

The above results ("crushed") were also compared with FODs obtained at the same scanning locations for the same sample, but scanning was started from the middle by polishing one side of the sample to the centerline ( $z/b \sim 0$ ). By scanning this way, the image quality is better for the core layer where fiber clumps are most likely to occur if scans is made from the sample surface ( $z/b \sim 1$ ). The comparison showed that the magnitudes of  $\langle a_{11} \rangle$  and  $\langle a_{33} \rangle$  agreed with each other (Figure 18 and Table 8). The reason why the image prepro-



cessing algorithm affects the  $\langle a_{33} \rangle$  more than the  $\langle a_{11} \rangle$  probably is due to the fact that the contribution of the clumps to  $\langle a_{11} \rangle$  is small compared with the total contributions of all fibers since most fibers are already aligned in the flow direction, but the clumps affect  $\langle a_{33} \rangle$  significantly because they create apparent fiber components with a strong z-component and they play a strong role in determining the magnitude of  $\langle a_{33} \rangle$ .

It is concluded that the preprocessor is necessary since results with a high confidence level require a larger amount of tracer fibers, which is more likely to create fiber clumps. The algorithm can also help to get rid of non-fiber image content such as dirt, voids, etc.

### **7.3.2 Results of Influence of Non-Uniform Voxel Sizes**

Two different voxel sizes in the optical sectioning direction (VoxSizeZ) were tested for the orthogonal sample, i.e., voxel sizes  $3.367 \times 1.993 \times 14.900$  and  $3.367 \times 1.993 \times 7.450 \mu\text{m}$  were used. Table 6 contains the orientation tensors as well as the unit vectors corresponding to the major axes of the ellipsoids.

**Table 6: Comparison of Tensor Components for Scans Using Different Voxel Sizes.**

	VoxSize.Z=14.900 $\mu m$				VoxSize.Z=7.450 $\mu m$			
	$a_{ij}$			$e_{major}$	$a_{ij}$			$e_{major}$
scan1	0.454	0.0890	0.2642	0.7088	0.4738	0.0969	0.2812	0.7303
		0.1418	0.1210	0.2429		0.1543	0.1331	0.2593
	sym		0.4042	0.6623	sym		0.3719	0.6319
scan2	0.4054	0.1170	0.2860	0.6574	0.3780	0.0990	0.2362	0.6656
		0.1952	0.1642	0.3334		0.2746	0.1235	0.2161
	sym		0.3993	0.6757	sym		0.3473	0.1211
scan3	0.4073	0.1388	0.2217	0.6681	0.4112	0.1455	0.2526	0.6619
		0.2349	0.1558	0.4089		0.2547	0.1866	0.4337
	sym		0.3577	0.1276	sym		0.3341	0.6114
scan4	0.3992	0.0843	0.2660	0.6799	0.3707	0.0981	0.2360	0.6672
		0.2241	0.1213	0.2927		0.2814	0.1374	0.2189
	sym		0.3767	0.6723	sym		0.3479	0.1139

Table 7 shows the variations of directions of these unit vectors from the average as well as the mean of the variations for the two different voxel sizes, which changes from 5.00 degrees to 4.26 degrees. Theoretically, if uniform voxel sizes are used, for example,  $2 \times 2 \times 2 \mu m$ , to represent fibers, there will not be any bias for the three orthogonal directions. The results indicated that changing the voxel size toward uniformity doesn't change the results significantly, but the image scanning time and storage space were doubled.

**Table 7: Comparison of Angle Differences from the Mean Direction for Scans Using Different Voxel Sizes.**

$\bar{\Delta}_i = \arccos(\vec{e}_i^{major} \cdot \vec{e}_{major})$	scan1	scan2	scan3	scan4	$\bar{\Delta} = \sqrt{(\Delta_i)^2 / 4}$
VoxelSize.Z=14.900	4.78	2.06	8.35	2.00	5.00
VoxelSize.Z=7.450	6.93	0.97	4.19	2.49	4.26

The above results lead to the conclusion that the present choice of voxel sizes has no significant influence on the accuracy of the FOD results but requires less storage space for the images.

#### 7.4 Estimates of Measurement Errors

Table 8. compares the results from the experiment and the theoretical error estimates for both the shell and the core layer, where  $d\langle a_{11} \rangle$  and  $d\langle a_{33} \rangle$  are the standard deviations of the ten measurements. For the experiment, 3 x 1 scans were repeated ten times and the mean and standard deviation were calculated. For the error estimate, the sensitivity coefficients were calculated using orientation and length information for each fiber using the equations derived (Eq. [22], section 5.4). Estimates of measurement errors were 5 degrees for both angles  $(\theta, \phi)$  and 15  $\mu m$  for the length  $l$ . It can be seen that the results obtained from experimental and theoretical estimates are consis-

tent in magnitude. This confirms that the measurement errors come mainly from the angles and the length.

**Table 8: Comparison of Experimental Uncertainty and Theoretical Error Estimates.**

Location	Results	$\langle a_{11} \rangle$	$d\langle a_{11} \rangle$	$\langle a_{33} \rangle$	$d\langle a_{33} \rangle$
shell layer	Experimental Uncertainty	0.866	0.009	0.020	0.007
	Theoretical Error Estimate		0.012		0.003
core layer	Experimental Uncertainty	0.440	0.017	0.111	0.020
	Theoretical Error Estimate		0.014		0.009

The contributions to the measurement errors due to uncertainty of length and angle are tabulated in Table 9. It can be seen that the in-plane x-y angle  $\phi$  contributes the most to the measurement uncertainty for both shell and core layers. The length contribution becomes significant for the core layer.

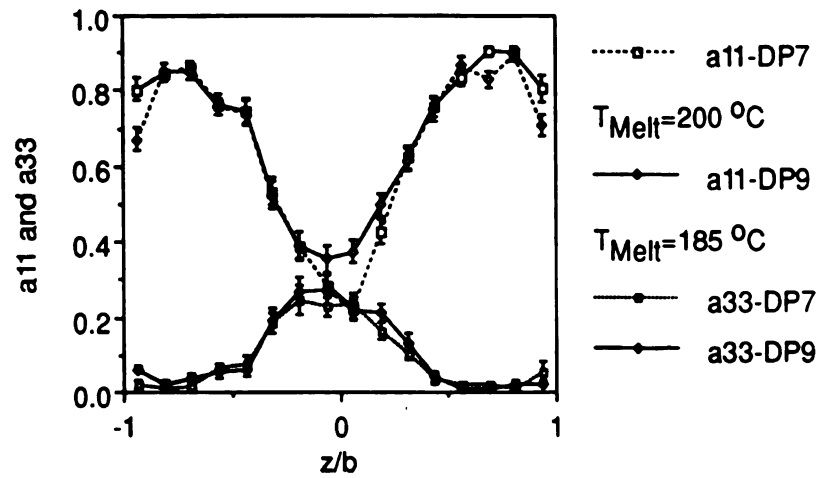
**Table 9: Error Contribution in Percentage.**

	$\sum_i \left( \frac{\partial}{\partial l_i} \langle a_{11} \rangle \right)^2 (\Delta l)^2$	$\sum_i \left( \frac{\partial}{\partial \theta_i} \langle a_{11} \rangle \right)^2 (\Delta \theta)^2$	$\sum_i \left( \frac{\partial}{\partial \phi_i} \langle a_{11} \rangle \right)^2 (\Delta \phi)^2$
shell layer	0.000064 (13.6%)	0.000006 (16.3%)	0.000080 (70.1%)
core layer	0.000026 (42.7%)	0.000031 (4.0%)	0.000133 (53.3%)

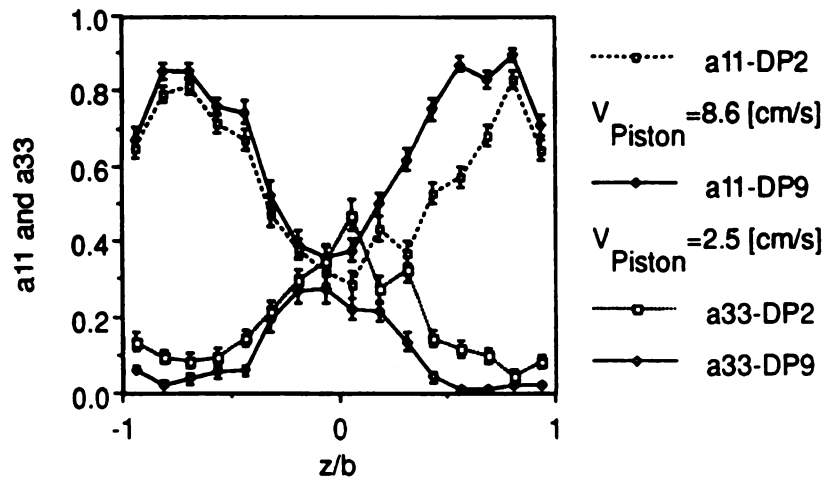
## **7.5 Results of Influence of Processing Parameters on FODs.**

### **7.5.1 Experimental Results of Influence of Processing Parameters on FODs.**

Samples were made under different processing conditions and comparisons of FODs are shown in Figure 21 (also see Thesis, Ladewig, 1993). The processing conditions for each samples are also shown in the same Figure. The first graph compares  $\langle a_{11} \rangle$  and  $\langle a_{33} \rangle$  of two samples produced with different melt temperatures while all other processing conditions were maintained the same. No significant differences in FODs were detected except for  $\langle a_{11} \rangle$  near the center. The other set of samples were made with different injection rates but all other conditions were the same. The FODs of the sample with the low injection rate showed a thicker shell layer, which could be explained by the formation of a solid boundary layer near the wall. For low injection speed, the solid boundary layer has more time to develop due to the heat transfer from the hot melt to the cold wall of the mold and a constrained flow channel is formed which favors high fiber alignment along the flow path and create a thicker shell layer. This observation agrees with the theoretical expectation.



Fiber Orientation of Specimen DP7 and DP9  
Melt Temperature Influence



Fiber Orientation of Specimen DP2 and DP9  
Injection Speed Influence; Pn=2.9

Figure 21. Influence of Temperature and Injection Speed on FODs.

FODs for samples produced using two different grades of PMMA were also compared as in Figure 22. PMMA produced by Eastman Kodak has higher molecular weight and viscosity, while PMMA provided by Dupont has lower

molecular weight and lower viscosity. It shows that the FODs of the sample made with high molecular weight has a thicker core layer which may be caused by the highly non-Newtonian behavior of the material where the shear thinning effect is significant. The solid curves are the through-thickness  $\langle a_{11} \rangle$  and  $\langle a_{33} \rangle$  components of  $3 \times 3$  scans taken at  $x/L \sim 0.5$  for sample produced with low viscosity PMMA and the error bars represent the standard deviation of the means ( $\langle a_{11} \rangle$  and  $\langle a_{33} \rangle$ ). The dotted lines are the average of FODs of

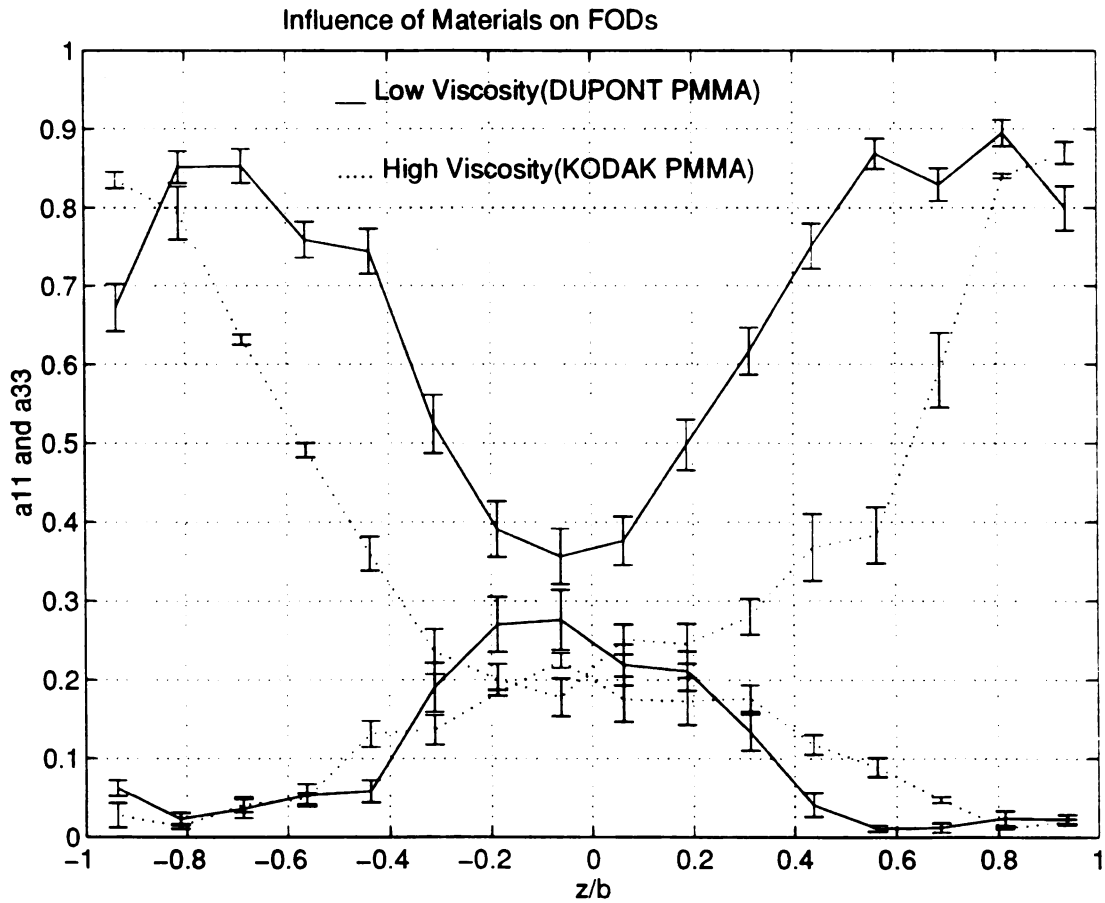


Figure 22. Material effect on FODs.

four samples made with high viscosity PMMA under the same conditions, the error bar represents the variation of the second order tensor components from sample to sample which shows good reproducibility of the results.

### **7.5.2 Results of Simulation of FOD Evolution During Mold Filling Process**

To understand the effects of material properties on the FODs, a simulation using the finite difference method was used to predict the evolution of FODs during the mold filling process.

Jeffery's equation is usually used to describe the motion of dilute suspensions in Newtonian fluids (Jeffery, 1923). Theoretical and experimental studies showed that non-Newtonian fluids (Gauthier, Goldsmith and Mason, 1971), non-linear flow fields (Shanker, Gillespie, and Guceri, 1991) have a measurable but relative small effect on the fiber orientation. The interaction between fibers appears to be the most significant "non-Jeffery" effect in these problems. Thus in this studies, Jeffery's equation was applied to describe the motion of fibers and Tucker's interaction model was used to modeled fiber-fiber interaction (Tucker, 1987).

The distribution function approach was used instead of working directly with

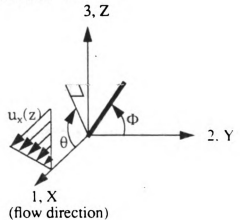


the second order tensor. The purpose was to acquire useful information about how the orientation of individual fibers evolve during the mold-filling process. A combination of Jeffery's equation and the Tucker interaction model (Tucker, 1987) yields the following equation of motion (rotation) for a single fiber within the flow field:

$$\dot{\theta} = \left[ \frac{r_e^2}{r_e^2 + 1} \right] \left\{ -\sin\theta \cos\theta \frac{\partial v_x}{\partial x} - (\sin\theta)^2 \frac{\partial v_x}{\partial y} + (\cos\theta)^2 \frac{\partial v_y}{\partial x} + \sin\theta \cos\theta \frac{\partial v_y}{\partial y} \right\} \\ - \left[ \frac{1}{r_e^2 + 1} \right] \left\{ -\sin\theta \cos\phi \frac{\partial v_x}{\partial x} + (\cos\theta)^2 \frac{\partial v_x}{\partial y} - (\sin\theta)^2 \frac{\partial v_y}{\partial x} + \sin\theta \cos\theta \frac{\partial v_y}{\partial y} \right\} \\ - \frac{C_I \dot{\gamma} \partial \Psi}{\Psi \partial \theta} \quad [26]$$

$$\dot{\phi} = \frac{\partial v_x}{\partial y} \left[ \frac{r_e^2 - 1}{r_e^2 + 1} \right] \sin\phi \cos\phi \sin\theta \cos\theta \quad [27]$$

where  $\theta$  is the angle of the fiber projection onto the x-z plane makes with the x-axis, and the velocity gradient is in the z direction, while  $\phi$  is the angle the fiber makes with the y-axis.  $C_I$  is the interaction coefficient and  $r_e$  the equivalent ellipsoidal axis ratio. The distribution function is  $\Psi$ .



Since the viscosity of polymer material depends on the shear rate and temperature, they will also influence the flow field (velocity profile) of the mold-filling process. The dependence of viscosity upon shear rate and temperature can be described by a power law:

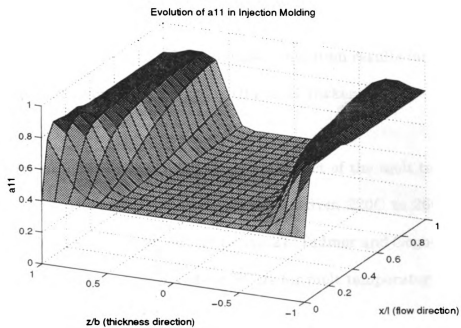
$$\eta(\dot{\gamma}, T) = \eta_o(T) \dot{\gamma}^{n-1} \quad [28]$$

where  $\dot{\gamma}$  is the magnitude of shear rate and  $n$  is the power law index. Different materials or same materials with different grades usually have quite different power law indices, and temperature can have moderate effect as well (Tadmor and Gogos, 1979).

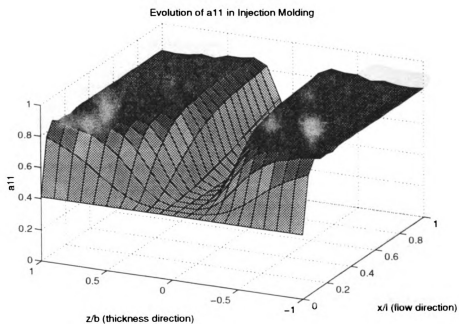
Two test cases were studied for different power law indices  $n$ :  $n=0.19$  (PMMA)

and  $n=0.65$  (Nylon6/6) with the same shear rate ( $\dot{\gamma} = \left| \frac{\partial v_x}{\partial y} \right| \sim 1000/s$ ) near the

wall. Random fiber orientation distribution was assumed for the initial state, and the time scale and a geometry similar to the operating conditions of the injection apparatus for this study were used. Figure 23 shows the evolution of  $\langle a_{11} \rangle$  through thickness along the flow direction for these two processes. The magnitude of  $\langle a_{11} \rangle$  near wall ( $|z/b| \sim 1$ ) increase quickly because the high shearing near the wall aligns the fibers in the flow direction, and fiber-fiber interaction disturb this alignment to some degree so that  $\langle a_{11} \rangle$  stays some where below 1.0 which corresponding to perfect alignment in the flow direction. The orientation distribution in the core region ( $z/b \sim 0$ ) doesn't change much since fibers experience no shearing in this region. It can be seen that



$n=0.19$  (PMMA)



$n=0.65$  (Nylon 6/6)

Figure 23. Material influence on FODs for PMMA and Nylon 6/6 (at  $T=220^{\circ}\text{C}$ ).

PMMA ( $n=0.19$ ) displays the influence of significant non-Newtonian behavior. The PMMA simulation shows a thicker core layer which agrees with our experimental finding (section 7.5.1), and the simulation results for Nylon6/6 is similar to the data from Tucker's group (Bay and Tucker, 1991).

Another comparison was made to explore the effect of the melt temperature. The melt temperature of PMMA was increased from 220C to 260C and the power law index changes from  $n=0.19$  to  $n=0.27$  (Tadmor and Gogos, 1979). No significant difference was observed for FODs for melt temperature 220C and 260C, as shown in Figure 24, which agreed with experimental observations (section 7.5.1).

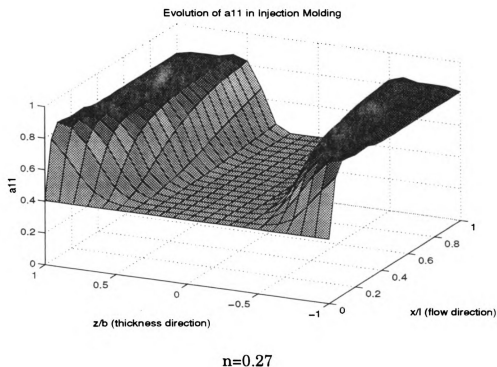


Figure 24. Evolution of FODs for  $T_{\text{melt}}$  (PMMA) at 260C.

The above results showed the influence of the effect of shearing on the fiber orientation distributions for isothermal processes. The effect of the injection speed is not shown here. Since the derivatives with respect to time and spatial coordinates in the equations of motion for the fibers are all first order, it indicates that the FODs will be the same for sample produced using different injection speed to a first order approximation (isothermal) (Tucker, 1984). If the heat transfer can not be neglected and isothermal condition is not satisfied, the injection speed will have some effect on FODs (see section 7.5.1).

Sophisticated software should be used if heat transfer, extensional flow and other factors such as complicated geometry of mold are needed for specific cases.

## **Chapter 8**

# **Conclusions and Recommendations for Future Work**

### **8.1 Calibrations**

Single fiber calibrations verified that the optical sectioning method can accurately measure the orientation (2 degrees error) and length (3% error) of individual fiber.

In the calibration using the random fiber orientation distribution created by PSEUDO, the FOD results given by the image analysis software suggested that the software can provide accurate and unbiased fiber orientation information even though non-uniform voxel sizes were used, the resulting FOD is very close to the known values of the second order tensor components ( $\langle a_{11} \rangle = \langle a_{22} \rangle = \langle a_{33} \rangle = 1/3$ ,  $\langle a_{12} \rangle = \langle a_{13} \rangle = \langle a_{23} \rangle = 0$ ) with less than 2% difference.

The calibration using the orthogonal sample also confirmed that the optical sectioning can provide accurate and consistent FOD results regardless of the scanning directions within 5 degrees for angle measurement and 3% error for length measurement.

## **8.2 Imaging Processing**

The experiment which utilized different voxel sizes demonstrated that non-uniform voxel sizes didn't significantly affect the FODs. The present choice of voxel size proved to be feasible in terms of accuracy and storage space consideration.

The incorporation of the image preprocessor is capable of removing fiber clumps and leaving good images intact, and the image processing time is reduced by about 30%. It could possibly shorten the fiber length for fibers that are close to the clumps but it is not significant. A more robust algorithm for the thinning program might be worthwhile to be developed to add more sophistication to deal with this problem.

### **8.3 Statistical Analysis**

Since the measurement errors of the optical sectioning system is relatively small (0.01 ~ 0.02) compared to the magnitude of the standard deviation of the mean (0.03 ~ 0.15) for the second order tensor components, it is appropriate to use the standard error to represent the uncertainty of the mean values  $\langle a_{ij} \rangle$ .

One of the major objectives of this project is to relate the processing parameters to the fiber orientation distributions. It is necessary to develop statistical criteria or measures for the comparison of FODs for samples produced under various conditions. Parametric or other approaches can be used for the comparisons.

### **8.4 Experimental Investigations of FODs.**

From the FOD results acquired experimentally, it was found that melt temperature did not affect the FODs significantly for the temperature range tested, but the injection speed showed some influence on the FODs. High injection speed tended to produce thicker core layer and thinner shell layer. The simulation results also supported these observations.

For the future work, the effects of mold geometry (converging, diverging) will



be an interesting problem to be studied.

The other way to further strengthen the plastic parts and reduce warpage is to use reinforcing ribs. The behavior of FODs within these ribs is a very important issue to achieve the goal of reinforcing. How the layout (orientation relative to the flow), sizing (size of ribs relative to the fiber length) of these ribs affect the FODs is virtually unknown experimentally.

### **8.5 Other Considerations**

One important factor that can make the optical sectioning technique more valuable is to develop other fiber/matrix combinations which utilize matrix materials that are popular for plastic reinforcing, such as polycarbonate.

This unique technique can also be applied to a wide variety of other applications. One interesting problem could be the thermal stress analysis. Fibers are incorporated into the plastics to provide enhancement of the mechanical properties such as strength and stiffness. They can also improve the thermal stability, such as reducing shrinkage and warpage. The FOD information is closely related to how much improvement can be obtained. The speed of optical sectioning allows fast comparison of FODs versus product performance and the nondestructive nature of the technique also allows other tests such as

mechanical tests to be carried out.

Our contact with Dr. Gilliland of the Statistics Department at MSU stimulated a discussion about the other way to calculate the standard errors for the tensor components. It will be interesting to study if there is any discrepancy between the results computed using current method and the method proposed by him for various conditions (sample size, distributions, etc.).

## Appendices

### A. Ratio Approach for Standard Error Calculation

$$\langle a_{11} \rangle = \frac{\sum_j L_j a_{11}^j}{\sum_j L_j} = \frac{\sum_j y_j}{\sum_j L_j}, \text{ where } y_j = L_j a_{11}^j;$$

$$\overline{a_{11}} = \frac{\bar{y}}{\bar{L}} = \text{ratio-of-average};$$

$$V(a_{11}) = \frac{1}{NL^2} [S_y^2 + \langle a_{11} \rangle^2 S_L^2 - 2 \langle a_{11} \rangle S_{yL}];$$

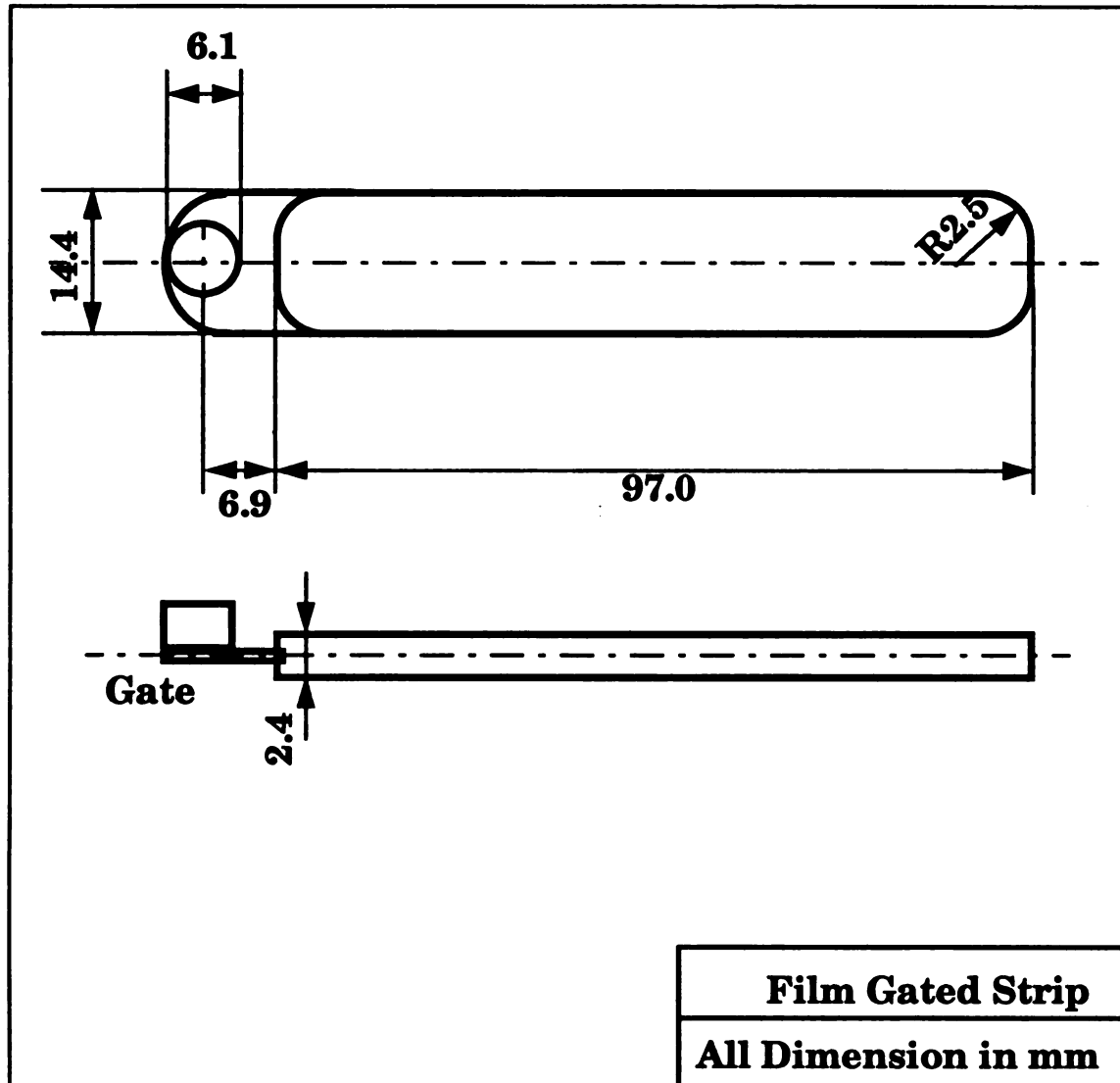
$$S_y^2 = \frac{1}{N-1} \sum_j (y_j - \bar{y})^2 = \frac{1}{N-1} \left[ \sum_j y_j^2 - N \bar{y}^2 \right];$$

$$S_L^2 = \frac{1}{N-1} \sum_j (L_j - \bar{L})^2 = \frac{1}{N-1} \left[ \sum_j L_j^2 - N \bar{L}^2 \right];$$

$$S_{yL} = \frac{1}{N-1} \sum_j (y_j - \bar{y}) (L_j - \bar{L}) = \frac{1}{N-1} \left[ \sum_j y_j L_j - N \bar{y} \bar{L} \right];$$

**Standard Error (standard deviation of the mean):**

$$SE(a_{11}) = 2.0 \sqrt{V(a_{11})} \text{ (with 95\% confidence level).}$$

**B. Specimen Geometry**

## List of References

- Wille, J.M. (1993). "Automated Measurement of 3-D Fiber Orientation Distribution in Injection molded Composites". *Ph.D Thesis*, Michigan State University, East Lansing.
- Ladewig, J. (1994). "3D Fiber Orientation of Short Fiber Reinforced Injection Molded Parts: Non-Dimensional Representation of Processing", *Diplomarbeit Thesis*, Michigan State University, East Lansing.
- Schöche, N. (1993). "Fiber Orientation in Transparent Short Fiber-Reinforced Thermoplastics". *Diplomarbeit Thesis*, Michigan State University.
- Bay, R.S. and Tucker III, C.L. (1991). "Fiber Orientation in Simple Injection Moldings. Part I: Theory and Numerical Methods". *Plastics and Plastic Composites: Material Properties, Part Performance, and Process Simulation*, MD-29, ASME, pp. 445-471.
- Bay, R.S. and Tucker III, C.L. (1991). "Fiber Orientation in Simple Injection Moldings. Part II: Experimental Results". *Plastics and Plastic Composites: Material Properties, Part Performance, and Process Simulation*, MD-29, ASME, pp. 445-471.
- Trevelyan, B.J. and Mason, S.G. (1951). "Particle Motions in Sheared Suspen-

sions. I. Rotations.”, *J. of Colloid Science*, Vol. 6, pp 354-367.

Advani, S.G. and Tucker III, C.L. (1985). “A Tensor Description of Fiber Orientation in Short Fiber Composite”. *SPE Technical Paper*, 31, pp.1113-1118.

Advani, S.G. and Tucker III, C.L. (1987). “The Use of Tensor s to Describe and Predict Fiber Orientation in Short Fiber Composites”. *Journal of Rheology*, 31, pp. 751-784.

Tadmor, Z. and Gogos, C.G. (1979). “Introduction to Polymer Processing”. *Principle of Polymer Processing*, John Wiley & Sons, New York, pp11-15.

Rayson, H.W. McGrath, G.C. and Collyer, A.A. (1986). “Fibers, Whiskers and Flakes for Composite Applications”. *Mechanical Properties of Reinforced Thermoplastics*. Elsevier Applied Science Publishers, pp. 29-64.

Chen, C.Y., and Tucker III, C.L. (1984). “Mechanical Property Prediction for Short Fiber/Brittle Matrix Composite”. *Journal of Reinforced Plastic Composite*, 3, pp. 120-129.

Christensen, R.M. (1979). *Mechanics of Composite Materials*, Wiley-Interscience, NewYork.

Fischer, G. and Eyerer, P (1988). “Measuring Spatial Orientation of Short Fiber Reinforced Thermoplastics by Image analysis”. *Polymer Composite*, 9(4), pp.297-304.

- Gleible W. (1990). "Process Control: Speed or Stress controlled Rheometry?", *Polymer Rheology and Processing*. Elsevier Applied Science Publishers. pp. 361-379.
- Bay, R.S. and Tucker III, C.L. (1992). "Stereological Measurement and Error Estimates for Three-Dimensional Fiber Orientation". *Polymer Engineering and Science*, Vol. 32, No.4, pp240-253.
- Hogg, R.V. and Craig, A.T. (1978). *Introduction to Mathematical Statistics*. Macmillan Publishing Co., Inc. pp122-180.
- Gauthier F., Goldsmith H.L. and Mason S.G. (1951). "Particle Motion in non-Newtonian Media. Part 1: Couette Flow", *Rheol. Acta* 10, pp. 344-364.
- Shanker R. Gillespie J.W. and Guceri S.I. (1991). "On the effect of nonhomogeneous Flow Fields on the Orientation Distribution and Rheology of Fiber Suspensions". *Polymer Eng. Sci.* 31, pp. 161-171.
- Advani S.G. and Tucker III C.L. (1993). "Processing of Short-Fiber Systems". *Flow and Rheology in Polymer Composites Manufacturing, Composite Materials Series 10*. Elsevier New York, pp. 147-202.
- Jeffery, G.B. (1923). "The Motion of Ellipsoidal Particles Immersed in a Vis-

cous Fluid", *Proc. Royal Society, Series A*, Vol. 102, pp. 161.

Gupta, M. and Wang, K.K. (1993). "Fiber Orientation and Mechanical Properties of Short-Fiber-Reinforced Injection-Molded Composites: Simulated Experimental Results", *Polymer Composites*, October 1993, Vol. 14, No.5, pp.367-382.

Folgar, F. and Tucker III, C.L. (1984). "Orientation Behavior of Fibers in Concentrated Suspensions.", *Journal of Reinforcing Plastics and Composites*, Vol. 3, April, 1984, pp. 98-119.



MICHIGAN STATE UNIV. LIBRARIES



31293013995455